MOLECULAR AND CELLULAR BIOLOGY, Sept. 2010, p. 4159–4174 Vol. 30, No. 17
0270-7306/10/$12.00 doi:10.1128/MCB.00235-10

Opposing Roles of Dnmt1 in Early- and Late-Stage Murine Prostate Cancer▽

Shannon R. Morey Kinney,[1]† Michael T. Moser,[1] Marien Pascual,[2] John M. Greally,[2] Barbara A. Foster,[1] and Adam R. Karpf[1]*

Department of Pharmacology and Therapeutics, Roswell Park Cancer Institute, Buffalo, New York 14263,[1] and Departments of Genetics (Computational Genetics) and Medicine, Albert Einstein College of Medicine, 1300 Morris Park Avenue, Bronx, New York 10461[2]

Received 28 February 2010/Returned for modification 17 April 2010/Accepted 14 June 2010

Previous studies have shown that tumor progression in the *t*ransgenic *a*denocarcinoma of *m*ouse *p*rostate (TRAMP) model is characterized by global DNA hypomethylation initiated during early-stage disease and locus-specific DNA hypermethylation occurring predominantly in late-stage disease. Here, we utilized *Dnmt1* hypomorphic alleles to examine the role of Dnmt1 in normal prostate development and in prostate cancer in TRAMP. Prostate tissue morphology and differentiation status was normal in *Dnmt1* hypomorphic mice, despite global DNA hypomethylation. *TRAMP*; *Dnmt1* hypomorphic mice also displayed global DNA hypomethylation, but were characterized by altered tumor phenotype. Specifically, *TRAMP*; *Dnmt1* hypomorphic mice exhibited slightly increased tumor incidence and significantly increased pathological progression at early ages and, conversely, displayed slightly decreased tumor incidence and significantly decreased pathological progression at advanced ages. Remarkably, hypomorphic *Dnmt1* expression abrogated local and distant site macrometastases. Thus, Dnmt1 has tumor suppressor activity in early-stage prostate cancer, and oncogenic activity in late stage prostate cancer and metastasis. Consistent with the biological phenotype, epigenomic studies revealed that *TRAMP*; *Dnmt1* hypomorphic mice show dramatically reduced CpG island and promoter DNA hypermethylation in late-stage primary tumors compared to control mice. Taken together, the data reveal a crucial role for Dnmt1 in prostate cancer and suggest that Dnmt1-targeted interventions may have utility specifically for advanced and/or metastatic prostate cancer.

Changes in DNA methyltransferase (Dnmt) expression and DNA methylation are observed in human prostate cancer (3, 38, 41). Of particular interest, genes with tumor suppressive function become hypermethylated and silenced, which correlates with the development of specific disease phenotypes (2, 3, 38). Although an association between prostate cancer and alterations in DNA methylation has been established, *in vivo* models are required to determine whether these changes functionally contribute to the disease. In this context, studies in which pharmacological inhibitors of Dnmts were shown to inhibit prostate cancer in murine models have proven informative (34, 56). However, it remains unknown whether genetic disruption of epigenetic components, such as Dnmts, also impacts prostate cancer development. This is a critical question since the pharmacological inhibitors of Dnmts have pleiotropic effects, including those unrelated to activation of methylation-silenced genes (21, 23, 31). Moreover, no studies to date have examined whether Dnmts or DNA methylation play roles in normal prostate development; this information is vital to fully understanding the effects that inhibiting DNA methylation may have on prostate cancer.

Dnmt1 is a maintenance DNA methyltransferase that propagates preexisting DNA methylation patterns in genomic DNA (44). Dnmt1 also is involved in *de novo* DNA methylation in cancer cells and interacts with other key epigenetic control molecules, including histone-modifying enzymes (11, 19). Murine models have been used to investigate the *in vivo* functions of Dnmt1. Complete genetic knockout of Dnmt1 is embryonic lethal in mice (29). However, hypomorphic expression of Dnmt1 allows murine development to proceed but causes global DNA hypomethylation and impacts cancer development and progression (7, 14, 28). Specifically, hypomorphic expression of Dnmt1 can lead to the development of lymphoma (14). Furthermore, crossing *Dnmt1* hypomorphic mice with murine tumor models alters tumor progression, resulting in either increased or decreased tumor development, depending on the disease stage and tissue site (1, 7, 53). For example, reduced expression of Dnmt1 dramatically decreases intestinal polyp formation in $Apc^{Min/+}$ mice, either alone or in combination with 5-aza-2′-deoxycytidine treatment (7, 27). However, it was later noted that reduced expression of Dnmt1 has a dual effect on intestinal cancer in $Apc^{Min/+}$ mice, in which the development of early stage intestinal microadenomas is accelerated, whereas the formation of adenomatous polyps is significantly reduced (53). In addition, $Apc^{Min/+}$ *Dnmt1* hypomorphic mice develop liver cancer associated with the loss of heterozygosity of *Apc* (53). Similarly, in *Dnmt1* hypomorphic mice crossed to $Mlh1^{-/-}$ mice, a dual effect was noted wherein mice developed fewer intestinal cancers but displayed increased T- and B-cell lymphomas (52). In addition, a recent study demonstrated that hypomorphic *Dnmt1* expression is associated with reduced squamous cell carcinoma of the tongue and esophagus, resulting in decreased invasive cancer (1). Taken together, the data

* Corresponding author. Mailing address: Roswell Park Cancer Institute, Elm and Carlton Streets, Buffalo, NY 14263. Phone: (716) 845-8305. Fax: (716) 845-8857. E-mail: adam.karpf@RoswellPark.org.
† Present address: New England Biolabs, 240 County Road, Ipswich, MA 01938-2723.
▽ Published ahead of print on 28 June 2010.

suggest that Dnmt1 has diverse effects on cancer development, which are dependent on tissue context and tumor stage.

TRAMP is a well-established transgenic prostate cancer model driven by prostate-specific expression of the simian virus 40 (SV40) T/t oncogenes (16). TRAMP mice are characterized by Dnmt mRNA and protein overexpression, altered DNA methylation, and altered gene expression during prostate cancer development (2, 33, 35, 37). Of the three enzymatically active Dnmts, Dnmt1 shows the greatest level of overexpression in TRAMP, and this correlates with Rb inactivation, a key genetic event driving prostate cancer in the model (37). Most critically, global DNA hypomethylation occurs during early and late disease stages, while DNA hypermethylation occurs primarily at late disease stages in TRAMP (35).

Here, we utilized *Dnmt1* hypomorphic mice and the TRAMP model to assess the role of DNA methylation in both normal prostatic development and prostate cancer. The *Dnmt1* hypomorphic mouse model used involves two different hypomorphic alleles (N and R), resulting in four genotypes with progressively reduced DNA methylation (*Dnmt1*$^{+/+}$, *Dnmt1*$^{R/+}$, *Dnmt1*$^{N/+}$, and *Dnmt1*$^{N/R}$) (7, 52). The N allele consists of a PGK-Neo insertion that deletes a portion of exon 4 of *Dnmt1*, resulting in severely reduced Dnmt1 expression, while the R allele involves a lacO insertion into intron 3 of *Dnmt1*, which partially reduces Dnmt1 expression (7, 52). Based on our previous work establishing the timing of DNA hypomethylation and DNA hypermethylation in TRAMP, we hypothesized that hypomorphic *Dnmt1* expression in TRAMP may have tumor-promoting effects at early disease stages and tumor-inhibitory effects at later stages of prostate cancer progression. Our data are consistent with this hypothesis and, more importantly, reveal a critical and unanticipated role for Dnmt1 in prostate cancer metastasis.

MATERIALS AND METHODS

***Dnmt1* hypomorphic mice and *TRAMP*; *Dnmt1* hypomorphic mice.** Animal studies were carried out under IACUC-approved protocols at Roswell Park Cancer Institute. *Dnmt1* hypomorphic mice were provided by Peter Laird (University of Southern California [USC] Norris Cancer Center) and have been described previously (7, 52). C57BL/6 *Dnmt1* hypomorphic mice carrying one hypomorphic allele and one wild-type (WT) (+) allele (*Dnmt1*$^{N/+}$ or *Dnmt1*$^{R/+}$) were mated to produce offspring that are C57BL/6 *Dnmt1*$^{+/+}$ (WT), *Dnmt1*$^{R/+}$, *Dnmt1*$^{N/+}$, or *Dnmt1*$^{N/R}$. Body, prostate, and urogenital tract (UG) weights were measured at euthanasia. To produce *TRAMP*; *Dnmt1* hypomorphic mice that are 50:50 C57BL/6-FVB, C57BL/6 *Dnmt1*$^{R/+}$ males were backcrossed to FVB homozygous TRAMP females for four generations, resulting in 93.75% FVB homozygous *TRAMP*; *Dnmt1*$^{R/+}$ mice. The resulting mice were crossed with C57BL/6 *Dnmt1*$^{N/+}$ mice to produce offspring that are 53.1:46.9 C57BL/6-FVB *TRAMP*; *Dnmt1* hypomorphic mice (of all four genotypes). Body, prostate, and UG weights were measured at euthanasia. Genotyping for *Dnmt1* and *Tag* alleles was completed on tail snip DNA extracted by using a Puregene DNA extraction kit (Gentra Systems, Minneapolis, MN), as described previously (7, 16). Primer sequences are available from the authors upon request.

qRT-PCR. RNA samples were extracted and used for quantitative real-time reverse transcription-PCR (qRT-PCR) analysis as described previously (35). The following genes were analyzed: *Dnmt1*, *Dnmt3a*, *Dnmt3b*, and *18S rRNA*. SYBR green absolute quantification was used to determine mRNA copy number, following normalization to 18S rRNA. PCRs were performed in triplicate. Primers were obtained from IDT (Coralville, IA) and were designed by using Primer3 or were previously reported (28, 46, 48). Primer sequences are available from the authors upon request.

Western blot analyses. Western blotting for Dnmt proteins was completed as described previously (35, 37). Ponceau S total protein stain was used to confirm equivalent protein loading.

Global DNA methylation analyses and mass array quantitative DNA methylation analysis (MAQMA). Quantification of 5-methyl-deoxycytidine (5mdC) levels was determined by liquid chromatography-electrospray ionization quadrapole mass spectrometry, as described previously (35, 50). Bisulfite pyrosequencing of the murine B1 repetitive DNA element was done as described previously (35). The mean methylation value of all sites was averaged for each sample. MAQMA was used to determine the methylation status of *Irx3*, *Cacna1a*, *Cdkn2a*, and *Nrxn2* as described previously (2, 10, 36).

HELP. HpaII tiny fragment enrichment by ligation-mediated PCR (HELP) analysis was performed as described previously (24, 39, 51). Six prostate samples were analyzed: (i) *Dnmt1*$^{+/+}$ (24 weeks), (ii) *Dnmt1*$^{N/R}$ (24 weeks), (iii) *TRAMP*; *Dnmt1*$^{+/+}$ (15 and 24 weeks), and (iv) *TRAMP*; *Dnmt1*$^{N/R}$ (15 and 24 weeks). To obtain representative samples from each experimental group, *Dnmt1*$^{+/+}$ and *Dnmt1*$^{N/R}$ prostate samples were selected based on those that were closest to the mean prostate weight and mean 5mdC level, for the corresponding genotype. Similarly, *TRAMP*; *Dnmt1*$^{+/+}$ and *TRAMP*; *Dnmt1*$^{N/R}$ prostate samples from 15-week-old mice were selected based on those that were closest to the median prostate weight and the mean 5mdC level for each genotype. *TRAMP*; *Dnmt1*$^{+/+}$ and *TRAMP*; *Dnmt1*$^{N/R}$ prostate samples from 24-week-old mice were selected based on those that were closest to the median disease score/median prostate weight and the mean 5mdC level for each genotype. Sequence features, including CpG islands and repetitive elements, were defined using the UCSC genome browser annotations for the mm8 mouse genome assembly, the same database used for designing the microarrays. The annotated sequences were then cross-correlated with the HELP data. We focused on the annotated RefSeq genes, defining promoters as the ±1-kb region flanking the transcription start site.

H&E and IHC staining. Five micron tissue sections were cut from paraffin-embedded blocks and mounted on slides. Slides were deparaffinized with xylene, rehydrated with alcohol, and equilibrated with Tris-phosphate buffer. Samples were stained with hematoxylin and eosin (H&E) or incubated with SV40 Tag antibody (1:400; catalog no. 554149; BD Pharmingen), AR (1:200; catalog no. 06-680; Millipore), p63 (1:100; catalog no. SC-8431; Santa Cruz), E-cadherin (1:500; catalog no. 610181; BD Pharmingen), smooth muscle actin (1:60; catalog no. V2258-0.2ML; Sigma-Aldrich), or Dnmt1 (1:50; catalog no. NB 100-264; Novus Biologicals) for immunohistochemistry (IHC), according to standard methods. Negative IHC controls utilized bovine serum albumin buffer alone, without primary antibody, during the primary antibody staining step. Tissue sections were scored for tumor grade using a compound Olympus XI-50 microscope equipped with QCapture imaging software. Two independent slides of each sample were analyzed.

Tumor incidence and tumor pathology measurements. Primary prostate tumor and macrometastatic tumor incidence were determined at necropsy by using a dissecting microscope. To measure prostate tumor stage, two slides of H&E-stained tissue sections 50 μm apart were analyzed for each mouse at 12, 15, and 24 weeks of age. The disease stage was assigned as described previously (20, 35). For comparison of the pathological grades, a disease index was calculated from the percentage of each pathological stage determined for the dorsal, lateral, and ventral prostate lobes according to the following formula: disease index = (% normal × 0) + (% PIN × 1) + (% well-differentiated [WD] × 2) + (% moderately differentiated [MD] × 3) + (% poorly differentiated [PD] × 4). One disease index value was calculated for each mouse based on the arithmetic average of the three prostate lobes, after averaging for the two slides analyzed. IHC of the SV40 tag was used to assess micrometastatic tumor incidence. Two slides (50 μm apart) of Tag-stained lymph node, kidney, lung, and liver tissue sections were analyzed for each mouse at 12, 15, and 24 weeks of age.

Statistics. Statistical analyses were performed by using the GraphPad Prism v5 (GraphPad Software, San Diego, CA). To test for differences between two groups with nonnormal distributions, we used a two-tailed nonparametric Mann-Whitney test. To test for differences in tumor incidence, we used the Fisher exact test. Disease index scores were compared by using the Mann-Whitney test. The figure legends contain specific information regarding the statistical analyses used for the indicated experiments.

RESULTS

Prostate development in *Dnmt1* hypomorphic mice. Survival defects in *Dnmt1*$^{N/R}$ hypomorphic mice have not been previously reported (7, 52). However, in our experiments, only

TABLE 1. Inheritance of *Dnmt1* hypomorphic alleles[a]

Genotype	No. of mice	Mendelian ratio	
		Expected	Observed
$Dnmt1^{+/+}$	53	0.25	0.34
$Dnmt1^{N/+}$	46	0.25	0.29
$Dnmt1^{R/+}$	49	0.25	0.31
$Dnmt1^{N/R}$	8	0.25	0.05

[a] F_1 offspring from cross of $Dnmt1^{R/+}$ and $Dnmt1^{N/+}$ C57BL/6 mice.

~20% of the expected amount of $Dnmt1^{N/R}$ mice were generated, whereas $Dnmt1^{R/+}$ and $Dnmt1^{N/+}$ mice were generated at expected levels (Table 1). These data suggest that $Dnmt1^{N/R}$ mice are near a critical threshold of DNA methylation required to sustain mouse development. To determine whether reduced Dnmt1 expression affects normal prostate development, we examined prostate weight and glandular morphology using H&E staining and the expression of several prostate differentiation markers by using IHC.

$Dnmt1^{N/R}$ mice showed decreased body weights at 15 and 24 weeks and reduced prostate weights at 15 weeks of age (Fig. 1A and B). However, following normalization to body weight, the prostate weights of mice from all four genotypes were similar (Fig. 1C). Thus, $Dnmt1^{N/R}$ mice appear to have a general survival and growth defect that does not specifically affect the prostate. Consistent with our findings, other strains of *Dnmt1* hypomorphic mice also have reduced body weight (1, 14).

Dnmt1 hypomorphic mouse prostates displayed a normal glandular morphology and general appearance (Fig. 2A). In addition, *Dnmt1* hypomorphic mice showed typical patterns of expression of several prostate differentiation markers, including p63 (basal cells), smooth muscle actin, androgen receptor (AR; luminal epithelial cells), and E-cadherin (luminal cells) (Fig. 2B). $Dnmt1^{N/R}$ mice showed a slight increase in cytosolic AR staining, but nuclear AR staining was retained (Fig. 2B). Male *Dnmt1* hypomorphic mice of all genotypes were fertile, suggesting that prostate function in these mice is normal (data not shown). Taken together, the data suggest that the prostates of surviving *Dnmt1* hypomorphic mice develop normally.

Dnmt expression and DNA methylation in *Dnmt1* hypomorphic mice. To define the Dnmt expression phenotype of *Dnmt1* hypomorphic mice, we measured *Dnmt1*, *Dnmt3a*, and *Dnmt3b* mRNA expression in the prostate and, as an additional control, in liver tissue by qRT-PCR. We analyzed mRNA as Dnmt protein expression is virtually undetectable in normal mouse prostate (35, 37). *Dnmt1* mRNA expression was reduced in both the prostates and the livers of *Dnmt1* hypomorphic mice, with the greatest decline in $Dnmt1^{N/R}$ mice (Fig. 3A and data not shown). In contrast, *Dnmt3a* and *Dnmt3b* displayed variable expression patterns, with a decrease in *Dnmt3b* expression in the prostate of $Dnmt1^{N/R}$ mice and upregulation of *Dnmt3a* and *Dnmt3b* in the liver of $Dnmt1^{N/R}$ mice at 24 weeks (Fig. 3A and data not shown).

The reduced expression of Dnmt1 in the prostate of $Dnmt1^{N/R}$ mice suggests that DNA methylation may be altered in these mice. To test this, we first measured global 5mdC levels and methylation of the *B1* repetitive element, as described previously (35, 50). Both measures of global DNA methylation were reduced in the prostates and livers of $Dnmt1^{N/R}$ mice but not in the other hypomorphic genotypes (Fig. 3B and C and data not shown). To more comprehensively evaluate DNA methylation in the $Dnmt1^{N/R}$ mouse prostate, we utilized the HpaII tiny fragment enrichment by ligation-mediated PCR assay (HELP), an epigenomic approach (24). We used HELP to compare DNA methylation profiles of prostates from $Dnmt1^{+/+}$ and $Dnmt1^{N/R}$ mice at 24 weeks of age. The proportions of hypermethylated HELP fragments in $Dnmt1^{+/+}$ and $Dnmt1^{N/R}$ mice were 78.7 and 76.7%, respectively, indicating a slight DNA hypomethylation effect (Fig. 3D). Consistent with this, a small loss in methylation occurred at gene bodies and repetitive DNA elements (Fig. 3D). Surprisingly, however, increased methylation was seen at promoters and CpG islands (Fig. 3D). This unexpected increase at normally hypomethylated regions suggests a compensatory DNA hypermethylation response in the $Dnmt1^{N/R}$ mouse prostate, possibly involving Dnmt3 enzymes. Analysis of hypomethylated genes identified by HELP in $Dnmt1^{N/R}$ mice revealed a number of genes previously found to be regulated by DNA

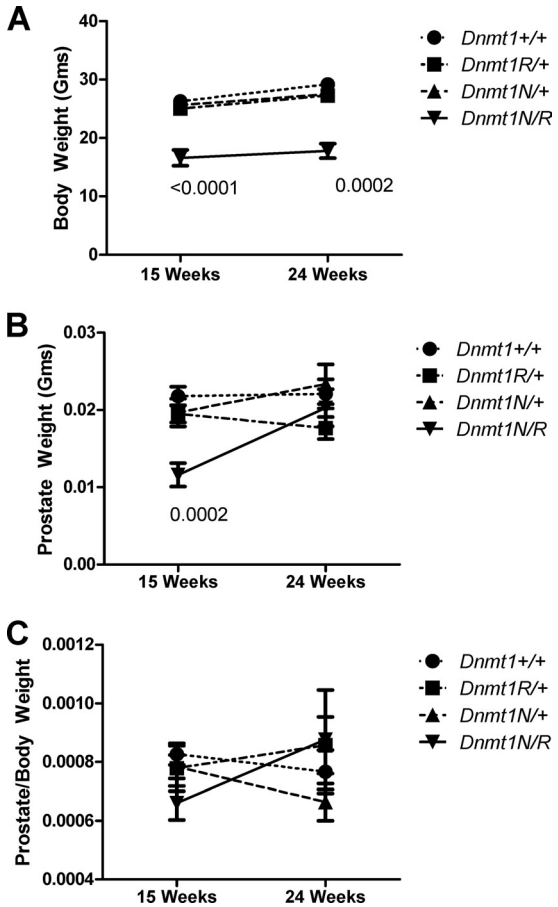

FIG. 1. Body and prostate weights of *Dnmt1* hypomorphic mice. (A) The body weights of 15- and 24-week-old mice of the indicated genotypes were determined at euthanasia. (B) The prostate weights of 15- and 24-week-old mice of the indicated genotypes were determined at euthanasia. (C) Prostate weight normalized to body weight. Error bars indicate the standard error. Mann-Whitney test P values of significant differences ($P \leq 0.05$), compared to $Dnmt1^{+/+}$ mice, are shown. In all panels, 8 to 15 mice were analyzed per group.

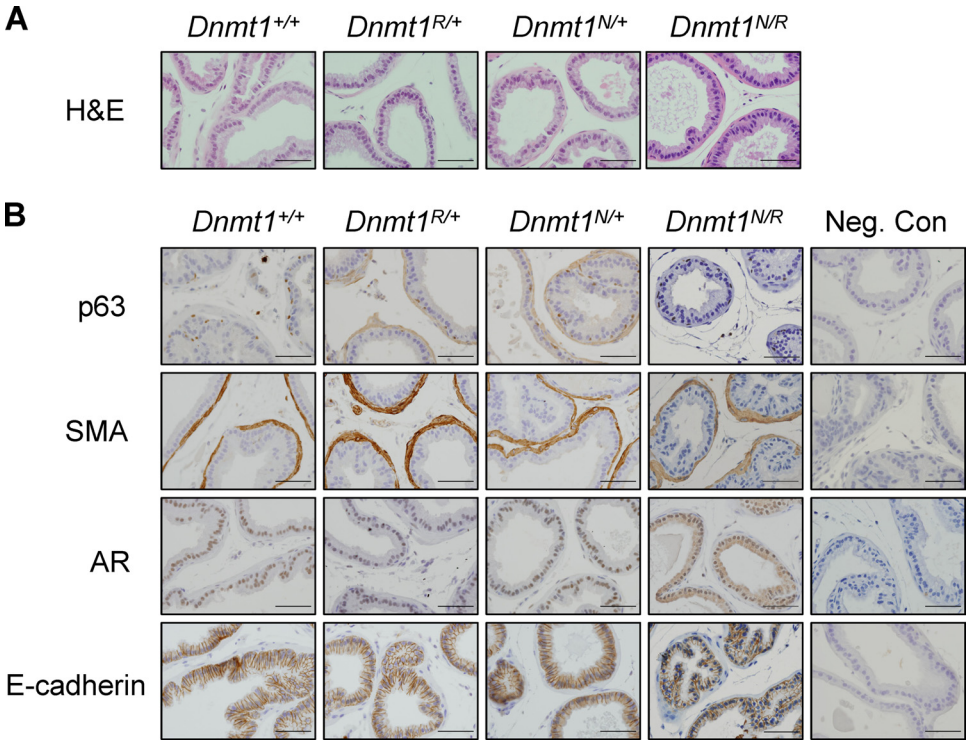

FIG. 2. Prostate tissue architecture and differentiation marker expression in *Dnmt1* hypomorphic mice. (A) H&E staining of lateral prostates from 15-week-old mice of the indicated genotypes was performed as described in Materials and Methods. (B) IHC staining of markers of prostate differentiation was performed on lateral prostates from 15-week-old mice of the indicated genotypes. The antibodies and conditions are described in Materials and Methods, and the negative control is shown at the right. Staining is shown for p63 (basal cell marker), smooth muscle actin (SMA; marker of the muscular layer surrounding glands), androgen receptor (AR; marker for luminal epithelial cells, with predominantly nuclear staining), and E-cadherin (marker for luminal epithelial cells, with predominantly plasma membrane staining). Scale bar, 100 μm.

methylation, including *Sohlh2*, *MyoG*, *PRAME*, and *p1a* (17, 32, 47, 49) (Table 2). Some of these genes can be classified as cancer-germ line antigens, a gene family methylated in most normal tissues (6). In addition, HELP identified a number of genes not previously known to be regulated by DNA methylation (Table 2). These data point to a complex DNA methylation phenotype in the *Dnmt1*$^{N/R}$ mouse prostate, characterized by global and gene specific DNA hypomethylation but also by DNA hypermethylation at specific genomic regions.

Generation of *TRAMP*; *Dnmt1* hypomorphic mice and analysis of Dnmt expression. *Dnmt1* hypomorphic mice are C57BL/6 (7, 52). In TRAMP, 50:50 C57BL/6-FVB mice present with tumors contained within the prostate (a finding more reflective of the human disease), rather than spreading to the seminal vesicles, which is observed in the pure C57BL/6 background (20). Thus, to generate *TRAMP*; *Dnmt1* hypomorphic mice in the 50:50 genetic background, we backcrossed *Dnmt1* hypomorphic mice to homozygous FVB TRAMP mice (see Materials and Methods). To minimize potential differences in tumor pathology due to strain effects, in all analyses we only compared age-matched littermates of the four *TRAMP*; *Dnmt1* hypomorphic genotypes: (i) *TRAMP*; *Dnmt1*$^{+/+}$, (ii) *TRAMP*; *Dnmt1*$^{R/+}$, (iii) *TRAMP*; *Dnmt1*$^{N/+}$, and (iv) *TRAMP*; *Dnmt1*$^{N/R}$. We collected samples from ~20 animals per genotype per time point. Due to the limited size of the prostate, at early ages (12 and 15 weeks), prostate tissues from half of the mice were embedded for histological analyses, and prostate tissues from the remaining mice were frozen for molecular analyses. At 24 weeks, prostate tissue was first embedded, and the remaining tissue was frozen for molecular studies; at this time point, individual tissues were usually large enough to use for both types of analyses.

To confirm specific knockdown of Dnmt1 in the target tissue, we measured Dnmt1, Dnmt3a, and Dnmt3b mRNA and protein expression in the prostates of *TRAMP*; *Dnmt1* hypomorphic mice at 12, 15, and 24 weeks. *Dnmt1* mRNA expression was significantly decreased in *TRAMP*; *Dnmt1*$^{N/R}$ mice at all three time points, whereas its levels were more variable in the *TRAMP*; *Dnmt1*$^{R/+}$ and *TRAMP*; *Dnmt1*$^{N/+}$ mice (data not shown). *Dnmt3a* and *Dnmt3b* mRNA expression was inconsistent, with the only significant change an increase in *Dnmt3a* in *TRAMP*; *Dnmt1*$^{N/+}$ mice at 24 weeks (data not shown). Similar to *Dnmt1* mRNA expression, Dnmt1 protein levels were decreased in *TRAMP*; *Dnmt1* hypomorphic mice (Fig. 4A and B). Although the most dramatic effect occurred in *TRAMP*; *Dnmt1*$^{N/R}$ mice, significant decreases were also observed in *TRAMP*; *Dnmt1*$^{R/+}$ mice and *TRAMP*; *Dnmt1*$^{N/+}$ mice at a minimum of one time point (Fig. 4B). IHC staining in prostate tissue confirmed the reduction of Dnmt1 expression in *TRAMP*; *Dnmt1*$^{N/R}$ mice, especially in poorly differentiated regions (data not shown). In contrast to Dnmt1, the Dnmt3a and Dnmt3b protein levels did not show a consistent pattern of

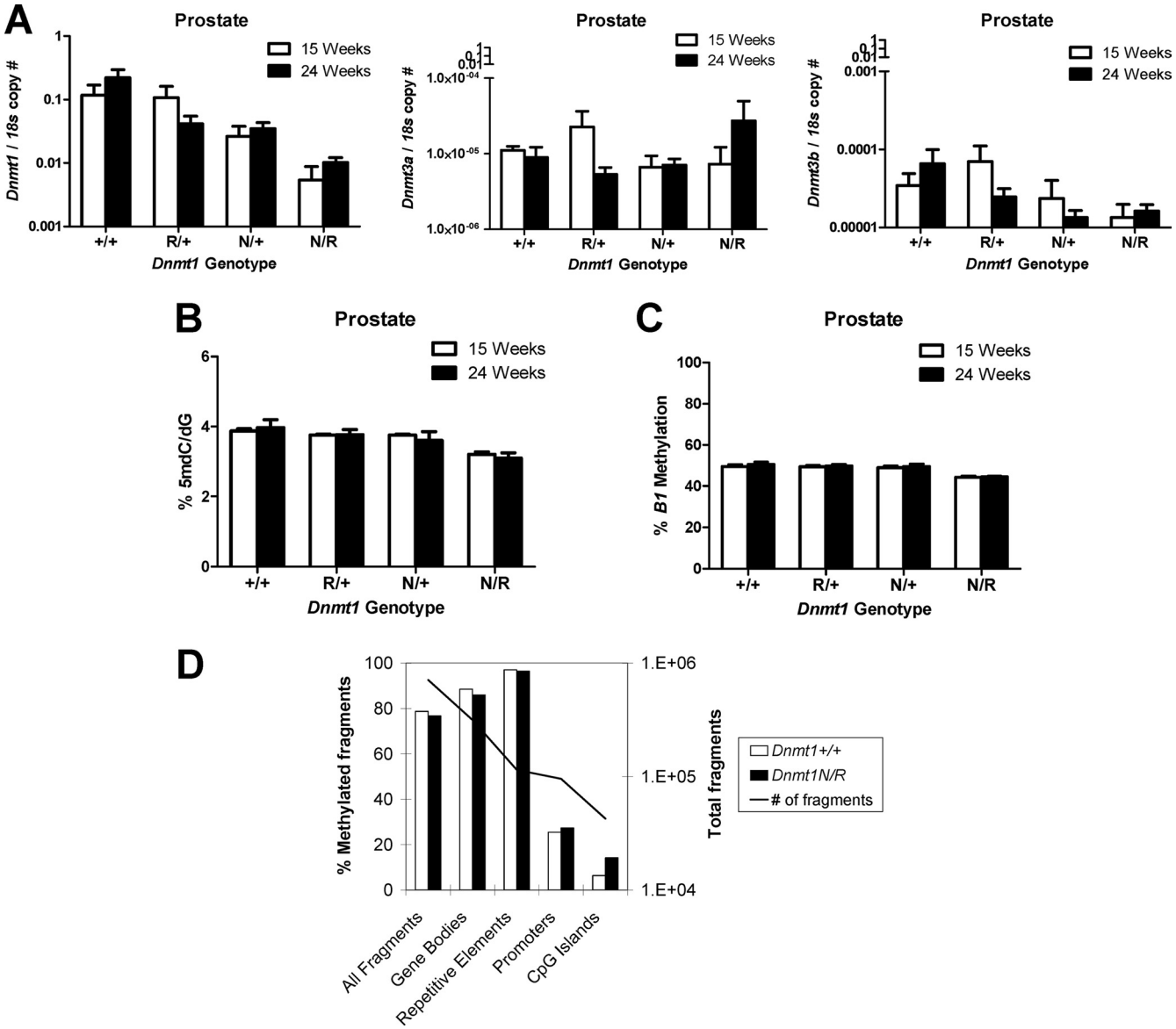

FIG. 3. *Dnmt* mRNA expression and global DNA methylation in the prostate of *Dnmt1* hypomorphic mice. (A) *Dnmt1* (left), *Dnmt3a* (center), and *Dnmt3b* (right) mRNA expression in prostate tissues from mice of the indicated genotypes, at 15 and 24 weeks of age, were measured by qRT-PCR as described in Materials and Methods. Three to six mice were analyzed per group, and the means and standard errors are plotted. (B) 5mdC levels in the prostate tissues from mice of the indicated genotypes, at 15 and 24 weeks of age, were measured by liquid chromatography-tandem spectrometry as described in Materials and Methods. Three to four mice were analyzed per group, and the means and standard errors are plotted. (C) The B1 repetitive element methylation levels in prostate tissues from mice of the indicated genotypes, at 15 and 24 weeks of age, were measured by sodium bisulfite pyrosequencing as described in Materials and Methods. Three to four mice were analyzed per group, and the means and standard errors are plotted. (D) HELP analysis of 24-week-old $Dnmt1^{+/+}$ and $Dnmt1^{N/R}$ mouse prostate. The total number of fragments analyzed are indicated by a line and plotted on the right axis, and the proportion of methylated fragments are indicated by columns and plotted on the left axis. HELP regions were subclassified as listed, as described in Materials and Methods.

altered expression in *TRAMP*; *Dnmt1* hypomorphic mice (Fig. 4C and D).

Since Dnmt expression is aberrant in TRAMP tumors as a function of the disease (35, 37), we additionally utilized liver as a control tissue to measure Dnmt expression in *TRAMP*; *Dnmt1* hypomorphic mice. Similar to the effects observed in the prostate, *Dnmt1* mRNA expression was significantly decreased in the liver of *TRAMP*; *Dnmt1* hypomorphic mice, whereas there were no consistent changes in *Dnmt3a* or *Dnmt3b* expression in this tissue (data not shown).

DNA methylation in *TRAMP*; *Dnmt1* hypomorphic mice. To assess DNA methylation in *TRAMP*; *Dnmt1* hypomorphic mice, we first measured global DNA methylation in prostate tissues. 5mdC levels were significantly decreased in *TRAMP*; $Dnmt1^{N/R}$ mouse prostates at all ages and in *TRAMP*; $Dnmt1^{N/+}$ mouse prostates at 15 and 24 weeks (Fig. 5A and C).

TABLE 2. Characteristics of the top 21 loci hypermethylated in 24-week-old *Dnmt1*$^{+/+}$ mice relative to *Dnmt1*$^{N/R}$ mice, identified by HELP[a]

Gene ID	Chromosome	Protein	Full name	Location of hypermethylated HELP fragment(s)		
				Promoter	Gene body	CpG island
NM_010401	10	Hal	Histidine ammonia lyase		X	
NM_027306	15	Zdhhc25	Zinc finger protein	X		
NM_011425	17	Sstr5	Somatostatin receptor 5	X		
NM_008938	17	Prph2	Peripherin 2	X		
NM_016977	18	Mc4r	Melanocortin receptor		X	
NM_031189	1	Myog	Myogenin		X	
NM_001011684	1	Nms	Neuromedin S	X		
NM_177191	2	Sycp2	Synaptonemal protein complex protein 2	X	X	X
NM_011784	2	Aplnr	Apelin receptor	X		
NM_028937	3	Sohlh2	Spermatogenesis and oogenesis specific basic helix-loop-helix 2		X	
NM_146255	4	Slc1a7	Solute carrier family transporter		X	
NM_031377	4	Pramel1	Preferentially expressed antigen in melanoma	X		
NM_031377	4	Pramel1	Preferentially expressed antigen in melanoma	X		X
NM_031377	4	Pramel1	Preferentially expressed antigen in melanoma	X		X
NM_001013751	5	Gm52	Syncytin a	X		
NM_001039678	5	Prhoxnb	Parahox cluster neighbor		X	
NM_177213	7	Abca15	ATP binding cassette transporter	X		
NM_001033316	7	Ffar3	Free fatty acid receptor 3	X		
NM_001033316	7	Ffar3	Free fatty acid receptor 3		X	
NM_019415	8	Slc12a3	Solute carrier family transporter	X	X	
NM_011635	X	Trap1a	Tumor rejection antigen p1a		X	

[a] That is, hypermethylated HELP fragments with a >1.6 log ratio (HpaII/MspI).

B1 methylation levels were unchanged in all genotypes at 12 weeks but were decreased in *TRAMP*; *Dnmt1*$^{N/R}$ mice at 15 and 24 weeks and in *TRAMP*; *Dnmt1*$^{N/+}$ mice at 15 weeks (Fig. 5D and F). Similarly, in liver, B1 methylation was decreased in *TRAMP*; *Dnmt1*$^{N/R}$ mice at 15 and 24 weeks and in *TRAMP*; *Dnmt1*$^{N/+}$ mice at 15 weeks (data not shown). These data indicate that hypomorphic *Dnmt1* expression in TRAMP causes global DNA hypomethylation in both tumor and normal tissues and that this effect is most dramatic in *TRAMP*; *Dnmt1*$^{N/R}$ mice.

We next examined whether hypomorphic *Dnmt1* expression alters locus-specific DNA hypermethylation in TRAMP tumors. Our prior studies, using restriction landmark genomic scanning (RLGS), identified loci that are hypermethylated in late-stage TRAMP tumors (2, 35, 37). Here, we used mass array quantitative methylation analysis (MAQMA) to analyze the methylation status of four loci identified by RLGS in our previous studies: *Irx3*, *Cacna1a*, *Cdkn2a*, and *Nrxn2* (2, 35, 37). *Irx3* displays 5′ region hypermethylation in TRAMP, whereas the other three genes display downstream gene body hypermethylation, suggesting that the causes of these epigenetic lesions may be distinct (2, 35, 37). MAQMA analysis of prostate samples from 24-week-old mice revealed that, relative to *TRAMP*; *Dnmt1*$^{+/+}$ mice, *Irx3* was hypomethylated in *TRAMP*; *Dnmt1*$^{N/+}$ and *TRAMP*; *Dnmt1*$^{N/R}$ mouse prostates (Fig. 6A). In contrast, the only significant methylation change at the other three loci was a loss of *Nrxn2* methylation in *TRAMP*; *Dnmt1*$^{R/+}$ mice (Fig. 6B to D). These data suggest that Dnmt1 may contribute to promoter DNA hypermethylation in TRAMP but may play a smaller role in downstream gene body hypermethylation.

To more comprehensively examine the effect of hypomorphic *Dnmt1* expression on DNA methylation in TRAMP, we conducted HELP analysis on *TRAMP*; *Dnmt1*$^{+/+}$ mice and *TRAMP*; *Dnmt1*$^{N/R}$ mice at 15 and 24 weeks of age (24). Sample selection was made as described in Materials and Methods. The experimental design allowed us to address how DNA methylation patterns change during progression from early-stage (15 weeks) to late-stage (24 weeks) prostate cancer, as well as to define the role of Dnmt1 in these changes. Overall, 81.1 and 86.0% of HELP fragments were methylated in *TRAMP*; *Dnmt1*$^{+/+}$ mice at 15 and 24 weeks, respectively, indicating a high degree of methylation that was further increased during tumor progression (Fig. 7A). In contrast, *TRAMP*; *Dnmt1*$^{N/R}$ mice showed a reduced level of methylation at 15 weeks (77.7%) that was only slightly increased at 24 weeks (78.5%) (Fig. 7A). The methylation level of *TRAMP*; *Dnmt1*$^{N/R}$ at 24 weeks was almost equivalent to *Dnmt1*$^{N/R}$ mice at this time point (78.7%; Fig. 3D). These data suggest that hypomorphic *Dnmt1* expression has a dramatic impact on DNA methylation genome-wide during tumor progression in TRAMP.

To determine the regions of the genome that were affected by Dnmt1 reduction, we further analyzed the HELP data to assess DNA methylation at repetitive DNA elements, CpG islands, gene bodies, and promoter regions (Fig. 7B to E). At repetitive DNA elements and gene bodies, *TRAMP*; *Dnmt1*$^{N/R}$ mice showed substantial DNA hypomethylation at 15 weeks, which was further evident at 24 weeks (Fig. 7B and C). This is consistent with the overall HELP fragment data (Fig. 7A) and likely reflects the fact that these regions are the most abundant class of HELP fragments (and genomic regions) analyzed. In contrast, and notably, CpG islands and promoter regions showed similar methylation in *TRAMP*; *Dnmt1*$^{+/+}$ mice and *TRAMP*; *Dnmt1*$^{N/R}$ mice at 15 weeks but highly divergent methylation at 24 weeks (Fig. 7D and E). This effect was

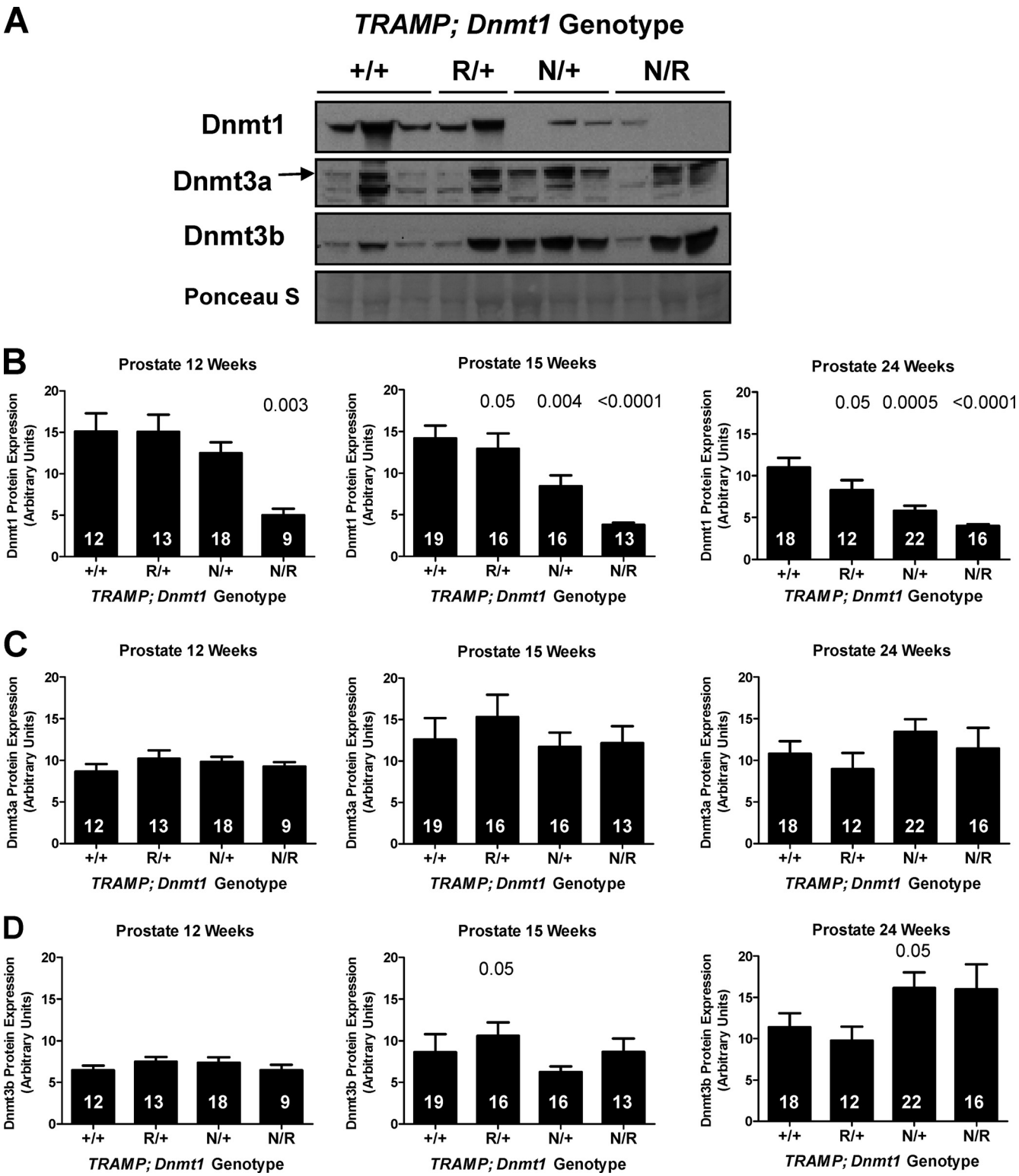

FIG. 4. Dnmt protein expression in prostates from *TRAMP*; *Dnmt1* hypomorphic mice. (A) Representative Western blots of Dnmt1, Dnmt3a, and Dnmt3b in prostate tissues from 24-week-old TRAMP mice of the indicated genotypes. The arrow indicates the position of Dnmt3a, as determined by Western analysis of Dnmt3a-null cell lines (data not shown). Ponceau S total protein staining was used to confirm equivalent protein input. (B) Dnmt1 protein expression in prostate tissues from TRAMP mice of the indicated genotypes and ages was determined by quantification of compiled Western blot data, as described in Materials and Methods. The number of samples analyzed per group is indicated on the bars, and means and standard errors are plotted. (C) Dnmt3a protein expression. (D) Dnmt3b protein expression. Mann-Whitney test P values of significant differences ($P \leq 0.05$), compared to *TRAMP*; *Dnmt1*$^{+/+}$ mice, are shown.

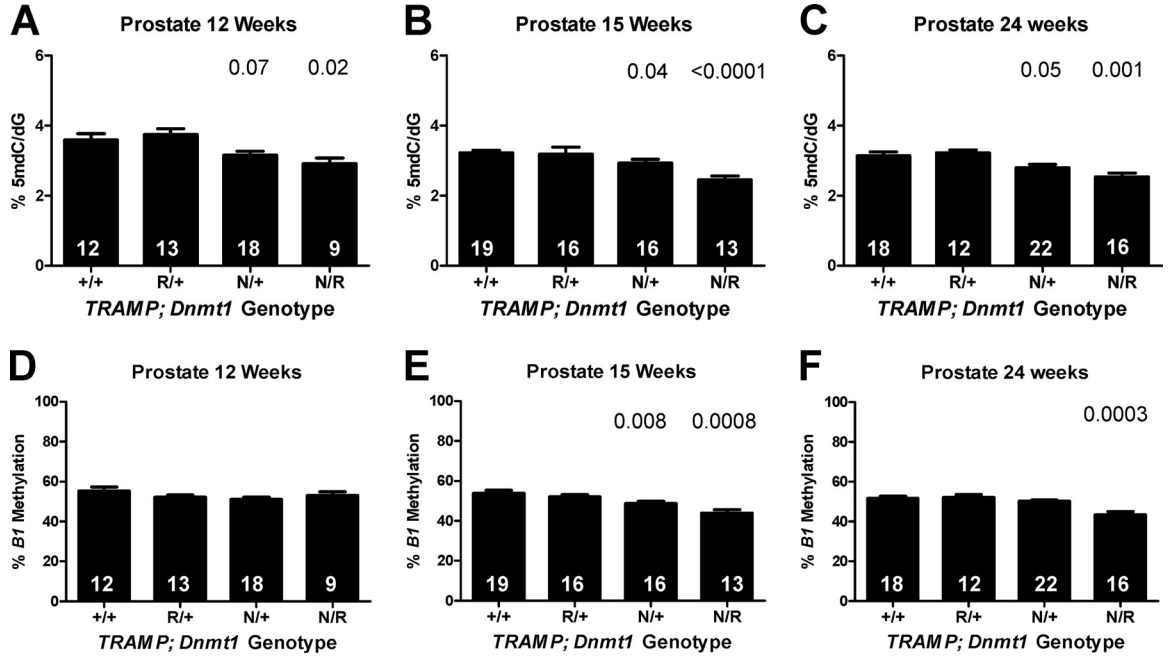

FIG. 5. Global DNA methylation in prostate tissues of *TRAMP*; *Dnmt1* hypomorphic mice. (A to C) 5mdC levels in prostate tissues from TRAMP mice of the indicated genotypes and ages was measured as described in Materials and Methods. The number of samples analyzed per group is indicated on the bars, and the mean and standard errors are plotted. (D to F) B1 repetitive element methylation levels in prostate tissues from mice of the indicated genotypes and ages was measured as described in Materials and Methods. The number of samples analyzed per group is indicated on the bars, and the means and standard errors are plotted. Mann-Whitney test *P* values of significant differences ($P \leq 0.07$), compared to *TRAMP*; *Dnmt1*$^{+/+}$ mice, are shown.

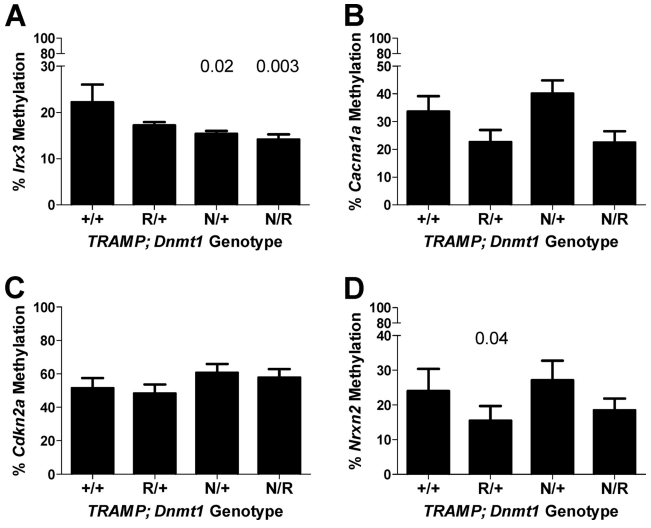

FIG. 6. Locus-specific DNA methylation in prostates from *TRAMP*; *Dnmt1* hypomorphic mice. MAQMA was used to determine locus-specific DNA methylation in prostate tissues from 24-week-old TRAMP mice of the indicated genotypes, as described in Materials and Methods. (A) *Irx3* 5′-region methylation; (B) *Cacna1a* gene body methylation; (C) *Cdkn2a* gene body methylation; (D) *Nrxn2* gene body methylation. In each panel, the number of samples analyzed per group was (from left to right) 18, 12, 22, and 16, and means and the standard errors are plotted. Mann-Whitney test *P* values of significant differences ($P \leq 0.05$), compared to *TRAMP*; *Dnmt1*$^{+/+}$ mice, are shown.

characterized by a robust increase in both CpG island and promoter region methylation in *TRAMP*; *Dnmt1*$^{+/+}$ mice at 24 weeks compared to 15 weeks, with no corresponding increase in *TRAMP*; *Dnmt1*$^{N/R}$ mice (Fig. 7D and E). The dramatic increase in CpG island methylation in *TRAMP*; *Dnmt1*$^{+/+}$ mice at 24 weeks is consistent with earlier studies showing that RLGS spot loss (which measures DNA methylation predominantly at CpG islands) is a late event during TRAMP tumor progression (35). Analysis of the genes showing the greatest degree of hypermethylation in *TRAMP*; *Dnmt1*$^{+/+}$ mice relative to *TRAMP*; *Dnmt1*$^{N/R}$ mice at 24 weeks revealed that most of the hypermethylated regions are in promoter CpG islands (Table 3). With the exception of a small subset of these genes, including *Csnk1g2*, *Ints6*, and *En1*, most of the identified genes are not previously known to be regulated by DNA methylation (25, 43, 45).

Primary tumor incidence and pathological stage in *TRAMP*; *Dnmt1* hypomorphic mice. The significantly altered DNA methylation patterns in *TRAMP*, *Dnmt1* hypomorphic mice (particularly in *TRAMP*; *Dnmt1*$^{N/R}$ mice) suggested that the tumor phenotype in these mice may be affected. To address this question, we analyzed several parameters in *TRAMP*; *Dnmt1* hypomorphic mice, including body, prostate, and UG tract weight, primary tumor incidence, and tumor pathology. Similar to *Dnmt1*$^{N/R}$ mice, *TRAMP*; *Dnmt1*$^{N/R}$ mice showed significantly reduced body weights relative to control mice (*TRAMP*; *Dnmt1*$^{+/+}$) (data not shown). However, after normalization to body weight, the *TRAMP*; *Dnmt1* hypomorphic mice did not show consistent changes in prostate weight compared to

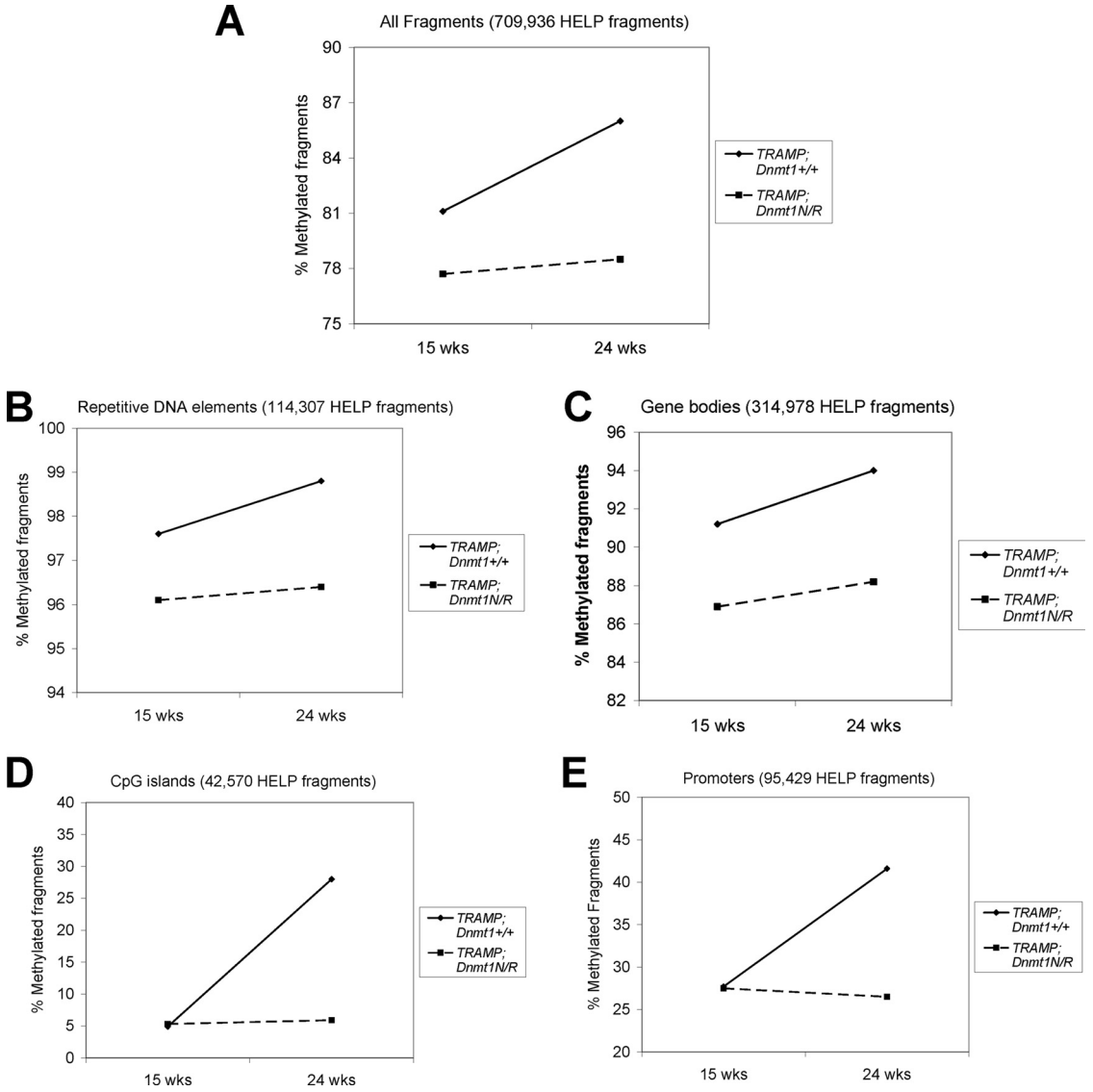

FIG. 7. HELP analysis of *TRAMP*; *Dnmt1*$^{+/+}$ and *TRAMP*; *Dnmt1*$^{N/R}$ mouse prostate at 15 and 24 weeks of age. Sample selection and HELP assays were performed as described in Materials and Methods. In all panels, the total number of HELP fragments analyzed is shown at top, and the proportion of fragments that are methylated is plotted. (A) All HELP fragments; (B) fragments in repetitive DNA elements; (C) fragments in gene bodies; (D) fragments in CpG islands; (E) fragments in promoter regions. HELP regions were subclassified as described in Materials and Methods.

the *TRAMP*; *Dnmt1*$^{+/+}$ mice (Fig. 8A). At early time points (12 and 15 weeks), *TRAMP*; *Dnmt1*$^{N/+}$ mice showed elevated primary tumor incidence compared to *TRAMP*; *Dnmt1*$^{+/+}$ mice (Fig. 8B). Similarly, *TRAMP*; *Dnmt1*$^{N/R}$ mice displayed an elevated tumor incidence at 15 weeks (Fig. 8B). However, these changes were not statistically significant (Table 4). Despite the increased tumor incidence at early time points, at 24 weeks of age, *TRAMP*; *Dnmt1* hypomorphic mice showed similar (i.e., *TRAMP*; *Dnmt1*$^{N/+}$ mice and *TRAMP*; *Dnmt1*$^{N/R}$ mice) or reduced (*TRAMP*; *Dnmt1*$^{R/+}$) primary tumor incidence compared to control mice (Fig. 8B and Table 4). These data suggested that hypomorphic *Dnmt1* expression may have opposing effects on prostate tumor formation, with a promotion effect at early stages and a suppressive effect at later stages of tumor progression.

To further define the effect of Dnmt1 reduction on prostate tumor development in TRAMP, we determined the pathological stage of primary tumors by examining H&E-stained prostate tissues. Tissue sections were scored for tumor stage (N, normal; PIN, prostatic intraepithelial neoplasia; WD, well differentiated; moderately differentiated; PD, poorly differentiated), and the percentage of tissue in each stage was determined as described previously (20). This method allowed us to calculate a disease index, which is based on the percentage of each pathological stage determined for each prostatic lobe. Disease index values represent the pathological stage averaged across three prostate lobes (dorsal, lateral, and ventral lobes). At 12 weeks of age, *TRAMP*; *Dnmt1*$^{N/R}$ mice had a significantly increased disease index value compared to *TRAMP*; *Dnmt1*$^{+/+}$ mice (Fig. 9A). At 15 weeks of age, all *TRAMP*; *Dnmt1* hypo-

TABLE 3. Characteristics of the top 27 candidate loci hypermethylated in 24-week-old *TRAMP*; *Dnmt1*$^{+/+}$ mice relative to *TRAMP*; *Dnmt1N/R* mice, identified by HELP[a]

Gene ID	Chromosome	Protein	Full name	Location of hypermethylated HELP fragment(s)		
				Promoter	Gene body	CpG island
NM_053014	10	Agpat3	1-Acylglycerol-3-phosphate *O*-acyltransferase 3	X		X
NM_134002	10	Csnk1g2	Casein kinase 1, gamma 2	X		X
NR_015372	11	Gm12166	Sft2d1 pseudogene	X	X	
NM_146047	13	Clptm1l	Cisplatin resistance related protein CRR9p	X		X
NM_207215	14	Mycbp2	MYC binding protein 2 (aka PAM in human)	X		X
NM_008715	14	Ints6	Integrator complex subunit 6 (DICE1, DDX26)		X	X
NM_172814	15	Lrp12	Low-density lipoprotein-related protein 12	X		X
NM_029457	16	Senp2	SUMO/sentrin-specific peptidase 2	X		X
NM_001081684	16	Zfp295	Zinc finger protein 295		X	X
NM_181397	17	Rftn1	Raftlin lipid raft linker 1	X		X
NM_007419	19	Adrb1	Adrenergic receptor, beta 1	X		X
NM_010133	1	En1	Engrailed	X		X
NM_023343	1	Ilkap	Integrin-linked kinase-associated serine/threonine phosphatase 2C	X		X
NM_030112	2	Rtf1	Rtf1, Paf1/RNA polymerase II complex component, homolog (*S. cerevisiae*)	X		X
NM_183023	2	Rims4	Regulating synaptic membrane exocytosis 4	X		X
NM_011098	3	Pitx2	Paired-like homeodomain transcription factor 2	X		
NM_001039090	3	Skil	SKI-like	X		X
NM_198960	4	Tcfap2e	Transcription factor AP-2, epsilon		X	X
NM_172890	6	Slc6a11	Solute carrier family 6 (neurotransmitter transporter, GABA), member 11	X		X
NM_177192	6	Dennd5b	DENN/MADD domain containing 5B	X		X
NM_010596	7	Kcna7	Potassium voltage-gated channel, shaker-related subfamily, member 7		X	X
NM_029332	7	Akap13	A kinase (PRKA) anchor protein 13		X	X
NM_001083118	8	Terf2	Telomeric repeat binding factor 2	X		X
NM_133765	8	Fbxo31	F-box protein 31	X		X
NM_001101502	8	Zfp703	Zinc finger protein 703	X		X
NM_030261	9	Sesn3	Sestrin 3	X		X
NM_211138	X	Pcyt1b	Phosphate cytidylyltransferase 1, choline, beta isoform		X[b]	

[a] Hypermethylated HELP fragments > 3.75 log ratio (HpaII/MspI).
[b] Alternative promoter.

morphic genotypes had increased disease index values compared to *TRAMP*; *Dnmt1*$^{+/+}$ mice (Fig. 9B). In contrast, at 24 weeks of age both *TRAMP*; *Dnmt1*$^{R/+}$ mice and *TRAMP*; *Dnmt1*$^{N/R}$ mice had decreased disease index values compared to *TRAMP*; *Dnmt1*$^{+/+}$ mice (Fig. 9C). These data suggest that Dnmt1 reduction accelerates the early stages of prostate tumor progression but inhibits the later stages of tumor progression in TRAMP mice.

Metastatic tumor formation in *TRAMP*; *Dnmt1* hypomorphic mice. One of the advantages of the TRAMP model is that primary prostate cancer progresses to local and distant site metastases, reminiscent of the human disease (15). This fact allowed us to investigate the impact of hypomorphic *Dnmt1* expression on metastatic tumor development *in vivo*, which, to our knowledge, has not been investigated previously (1, 7, 9, 14, 52). Initially, we examined macrometastatic tumor growth at necropsy by visual inspection of target tissues with a dissecting microscope. A negligible level of metastases developed in TRAMP mice at early time points (12 and 15 weeks), as expected (Fig. 8C and Table 4). However, at 24 weeks, 30% of *TRAMP*; *Dnmt1*$^{+/+}$ mice developed metastatic tumors (Fig. 8C and Table 4). Strikingly, macrometastatic tumor development was reduced in all three *TRAMP*; *Dnmt1* hypomorphic mouse genotypes, with a complete elimination of macrometastases in *TRAMP*; *Dnmt1*$^{N/R}$ mice (Fig. 8C and Table 4). Both local and distant site macrometastases were reduced in *Dnmt1* hypomorphic mice; these reductions are statistically significant in *TRAMP*; *Dnmt1*$^{N/R}$ mice (Table 4).

To determine the stage at which hypomorphic *Dnmt1* expression impacts metastatic tumor development, we next assessed micrometastatic lesions using IHC staining for Tag on lymph node, liver, lung, and kidney tissues, the common sites of metastases in TRAMP (18, 20). Consistent with the macrometastasis data, only a negligible level of micrometastatic tumors was present at 12 and 15 weeks of age in all genotypes (Table 5). However, at 24 weeks, 40 and 15% of *TRAMP*; *Dnmt1*$^{+/+}$ mice developed local and distant micrometastatic tumors, respectively (Table 5). Interestingly, the incidence of local micrometastatic tumors at 24 weeks was similar in *TRAMP*; *Dnmt1*$^{+/+}$ mice, *TRAMP*; *Dnmt1*$^{N/+}$ mice, and *TRAMP*; *Dnmt1*$^{N/R}$ mice but was reduced in *TRAMP*; *Dnmt1*$^{R/+}$ mice (Table 5). In contrast, all strains of *Dnmt1* hypomorphic mice showed reduced micrometastatic tumors at distant sites; this effect was most dramatic in *TRAMP*; *Dnmt1*$^{N/R}$ mice, in which no lesions were observed (Table 5). These findings were consistent with the complete absence of distant macro-metastatic tumors in *TRAMP*; *Dnmt1*$^{N/R}$ mice (Table 4) and reveal that Dnmt1 plays a critical role in establishing distant site metastases in TRAMP.

Finally, to determine whether reduction in circulating androgens in the *TRAMP*; *Dnmt1*$^{N/R}$ mice accounted for the observed inhibitory effect on metastatic tumor growth at 24

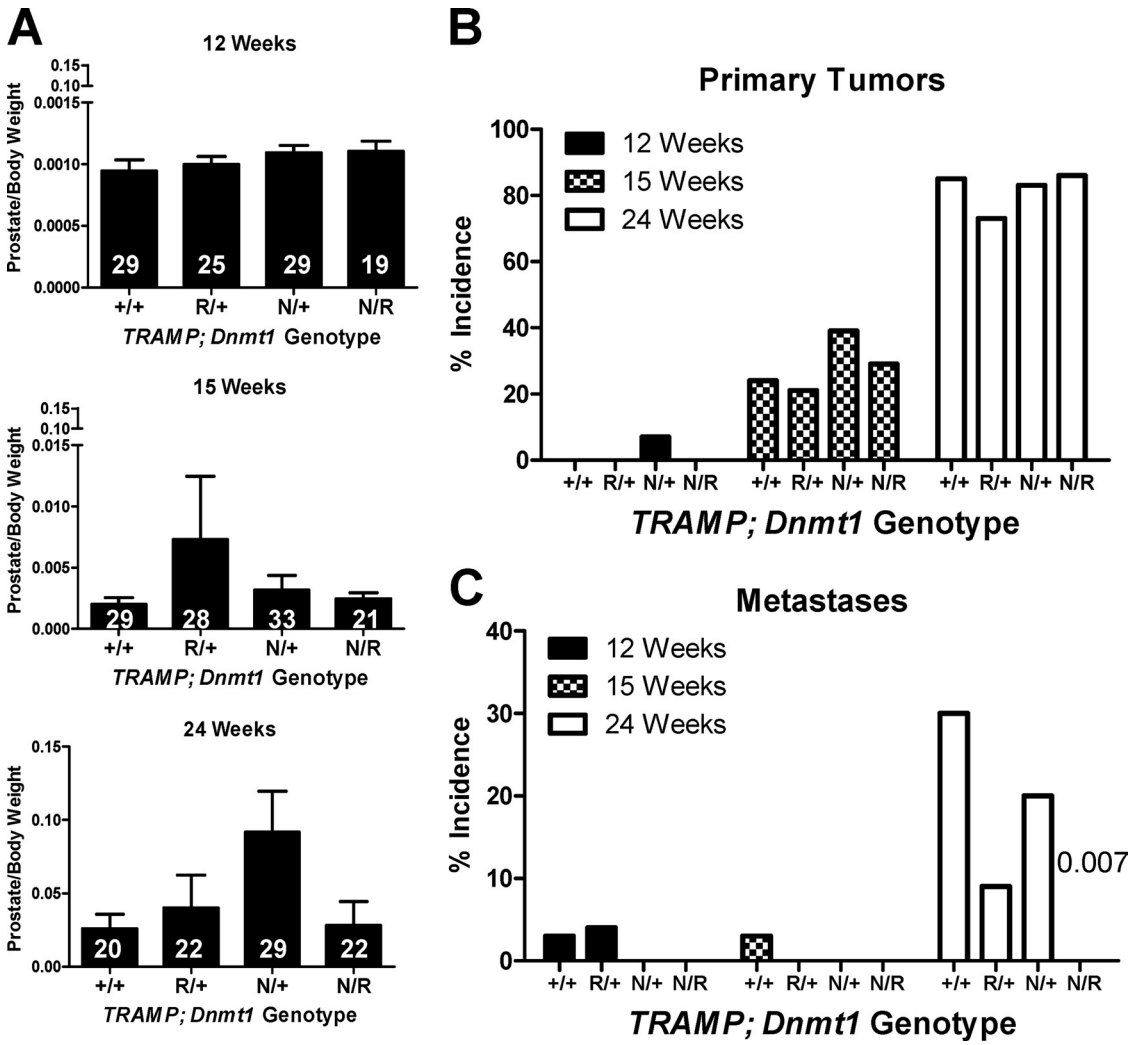

FIG. 8. Prostate weight and tumor incidence in *TRAMP*; *Dnmt1* hypomorphic mice. (A) Prostate weights (normalized to body weight) of TRAMP mice of the indicated genotypes were determined at necropsy at the indicated ages. The number of samples analyzed per group is indicated on the bars, and the means and standard errors are plotted. No significant differences ($P \leq 0.05$; Mann-Whitney test) were observed. (B) The primary tumor incidence of TRAMP mice of the indicated genotypes was determined at necropsy at the indicated ages. Each bar indicates the mean of a sample group where the number of samples analyzed per group is the same as in panel A. No significant differences ($P \leq 0.05$; Fisher exact test) were observed. (C) The macrometastatic tumor incidence of TRAMP mice of the indicated genotypes was determined at necropsy at the indicated ages. Each bar indicates the mean of a sample group where the number of samples analyzed per group is the same as in panel A. Fisher exact test *P* values of significant differences ($P \leq 0.05$), compared to *TRAMP*; $Dnmt1^{+/+}$ mice, are shown.

weeks, we conducted two independent tests. First, we measured UG weight, which would be expected to show a dramatic decrease in mice with reduced circulating androgens due to the strict dependence of the rodent urogenital tract on testosterone for growth (26). As shown in Fig. 10A, *TRAMP*; $Dnmt1^{+/+}$ mice and *TRAMP*; $Dnmt1^{N/R}$ mice show very similar UG sizes, after normalization to body weight, at all three time points (12, 15, and 24 weeks). As a second test, we measured nuclear AR staining, since nuclear localization of AR is dependent on androgens (4). We stained 17 *TRAMP*; $Dnmt1^{+/+}$ and 22 *TRAMP*; $Dnmt1^{N/R}$ mouse prostate and seminal vesicle sections (two slides per animal) with AR antibody for IHC, as described in Materials and Methods. The slides were deidentified, and nuclear AR staining was scored (as yes or no [Y/N]). The resulting data revealed no difference in nuclear AR staining between the two genotypes (data not shown; representative AR IHC staining of seminal vesicles is shown in Fig. 10B). Taken together, these data suggest that it is highly unlikely that alterations in circulating androgens account for the dramatic reduction of metastatic tumor growth observed in *TRAMP*; $Dnmt1^{N/R}$ mice.

DISCUSSION

Dnmt1 in prostate development and DNA methylation. In wild-type mice, hypomorphic *Dnmt1* expression did not alter the general morphology of the prostate, nor did it appear to alter its differentiation state. However, $Dnmt1^{N/R}$ mice (which showed the lowest level of Dnmt1 expression and greatest degree of DNA hypomethylation) had a significant

TABLE 4. Primary and metastatic tumor incidence in *TRAMP*; *Dnmt1* hypomorphic mice[a]

Time (in wks) and TRAMP *Dnmt1* genotype	*n*	Primary tumors		Total metastatic tumors		Local metastatic tumors		Distant metastatic tumors	
		%	*P*	%	*P*	%	*P*	%	*P*
12									
+/+	29	0	NA	3	NA	0	NA	3	NA
R/+	25	0	1	4	1	0	1	4	1
N/+	29	7	0.49	0	1	0	1	0	1
N/*R*	19	0	1	0	1	0	1	0	1
15									
+/+	29	24	NA	3	NA	0	NA	3	NA
R/+	28	21	1	0	1	0	1	0	1
N/+	33	39	0.28	0	1	0	1	0	1
N/*R*	21	29	0.75	0	1	0	1	0	1
24									
+/+	20	85	NA	30	NA	20	NA	20	NA
R/+	22	73	0.46	9	0.12	9	0.40	4.5	0.17
N/+	29	83	1	21	0.51	21	1	3	0.14
N/*R*	22	86	1	0	0.007*	0	0.04*	0	0.04*

[a] Fisher exact test *P* values, compared to *TRAMP*; $Dnmt1^{+/+}$ mice, were determined. "Local" refers to lymph node metastases; "distant" refers to liver, lung, or kidney metastases. *, significant difference ($P \leq .05$). NA, not applicable. *n*, number of mice.

survival defect, as evidenced by a 5-fold decrease from the expected Mendelian ratio. Surviving $Dnmt1^{N/R}$ mice also had reduced body weights. These data provide evidence that Dnmt1 is required for normal vertebrate development and are in agreement with previous data showing that *Dnmt1* knockout mice are embryonic lethal and that *Dnmt1* knockdown zebrafish show reduced survival (29, 42). Our data suggest that the level of Dnmt1 expression in $Dnmt1^{N/R}$ mice is close to the threshold required for normal murine development. Importantly, however, the defects observed in $Dnmt1^{N/R}$ mice did not appear to specifically impact the development of the prostate. Since *Dnmt3a* and *Dnmt3b* expression was retained in *Dnmt1* hypomorphic mice, it is reasonable to hypothesize that these enzymes may compensate for Dnmt1 reduction in the surviving $Dnmt1^{N/R}$ mice. Most important for the present study, the apparently normal development of the prostate in surviving *Dnmt1* hypomorphic mice suggests that this genetic model is valid for assessing the impact of reduced Dnmt1 expression on prostate cancer.

As expected, $Dnmt1^{N/R}$ prostate and livers had reduced levels of 5mdC and *B1* repetitive element methylation, which are measures of global DNA methylation status. In addition, HELP analyses revealed slight genome-wide hypomethylation in the $Dnmt1^{N/R}$ prostate. However, HELP also revealed a more complicated pattern of DNA methylation alterations in the $Dnmt1^{N/R}$ prostate. Although a number of genes were identified that become hypomethylated in the $Dnmt1^{N/R}$ prostate, these events frequently occurred outside of CpG islands. Moreover, unexpectedly, CpG island regions overall were hypermethylated in the $Dnmt1^{N/R}$ prostate compared to $Dnmt1^{+/+}$ mice. It is possible that this effect reflects compensatory epigenetic mechanisms (possibly mediated by Dnmt3 enzymes) that act in response to global DNA hypomethylation. Dual or combinatorial Dnmt disruption approaches *in vivo* could be used to test this idea. Potentially, this type of feedback response could explain the frequent coexistence of global DNA hypomethylation and CpG island hypermethylation observed in human cancer.

Dnmt1 and DNA methylation alterations during prostate cancer progression. Tumor progression in TRAMP is characterized by two major alterations in DNA methylation: (i) global hypomethylation appearing at early stages that becomes more pronounced at later stages and (ii) locus-specific CpG island hypermethylation, which is chiefly observed in the late stages of prostate cancer development (35). In *TRAMP*; $Dnmt1^{N/R}$ mice, these two alterations were exacerbated or inhibited, respectively. By 15 weeks of age, 5mdC and *B1* methylation levels in the prostates of *TRAMP*; *Dnmt1* hypomorphic mice were significantly reduced. In agreement with this, HELP analysis revealed genome-wide DNA hypomethylation in *TRAMP*; $Dnmt1^{N/R}$ mice at 15 weeks. The hypomethylating effect was seen specifically at repetitive DNA elements and gene bodies at this time point but was not seen at the promoters or CpG islands. A likely explanation for the lack of hypomethylation at the CpG islands and promoters at 15 weeks in *TRAMP*; $Dnmt1^{N/R}$ mice is that these regions are largely hypomethylated at baseline and the aberrant hypermethylation of these regions had not occurred to significant levels at this time. In contrast, at 24 weeks, *TRAMP*; $Dnmt1^{+/+}$ mice showed dramatic increases in both CpG island and promoter hypermethylation. Remarkably, these changes appeared to be completely abrogated in *TRAMP*; $Dnmt1^{N/R}$ mice, supporting a major role for Dnmt1 in CpG island and promoter region DNA hypermethylation during prostate cancer progression. The current data set does not allow us to resolve whether Dnmt1 is involved in *de novo* or maintenance methylation at these hypermethylated regions.

Our prior work using RLGS identified two general categories of DNA hypermethylation events in TRAMP: one in which promoter methylation is correlated with gene repression and a second in which gene body methylation is associated with increased gene expression (2, 35, 37). Interestingly, in *TRAMP*; *Dnmt1* hypomorphic mice it appeared that promoter hypermethylation is inhibited (illustrated by *Irx3*), whereas downstream hypermethylation was inconsistently affected (as illustrated by *Cacna1a*, *Cdkn2a*, and *Nrxn2*). This suggests that Dnmt1 may be primarily involved in initiating or maintaining aberrant promoter hypermethylation, with a less important role in catalyzing downstream gene DNA hypermethylation in TRAMP. Further studies are necessary to determine whether hypomorphic *Dnmt1* expression alters the expression of hypermethylated gene targets in TRAMP.

Opposing roles for Dnmt1 in early- and late-stage primary prostate cancer. The dual nature of the DNA methylation changes observed in TRAMP revealed in our previous studies (i.e., global hypomethylation appearing at early stages, CpG island hypermethylation at late stages) led us to hypothesize that hypomorphic *Dnmt1* expression may accelerate early-stage prostate tumor development and, conversely, inhibit late-stage prostate cancer. Our data support this hypothesis. At 12 and 15 weeks of age, *TRAMP*; *Dnmt1* hypomorphic mice showed slightly increased primary prostate tumor incidence, as well as significantly increased pathological stage (i.e., the dis-

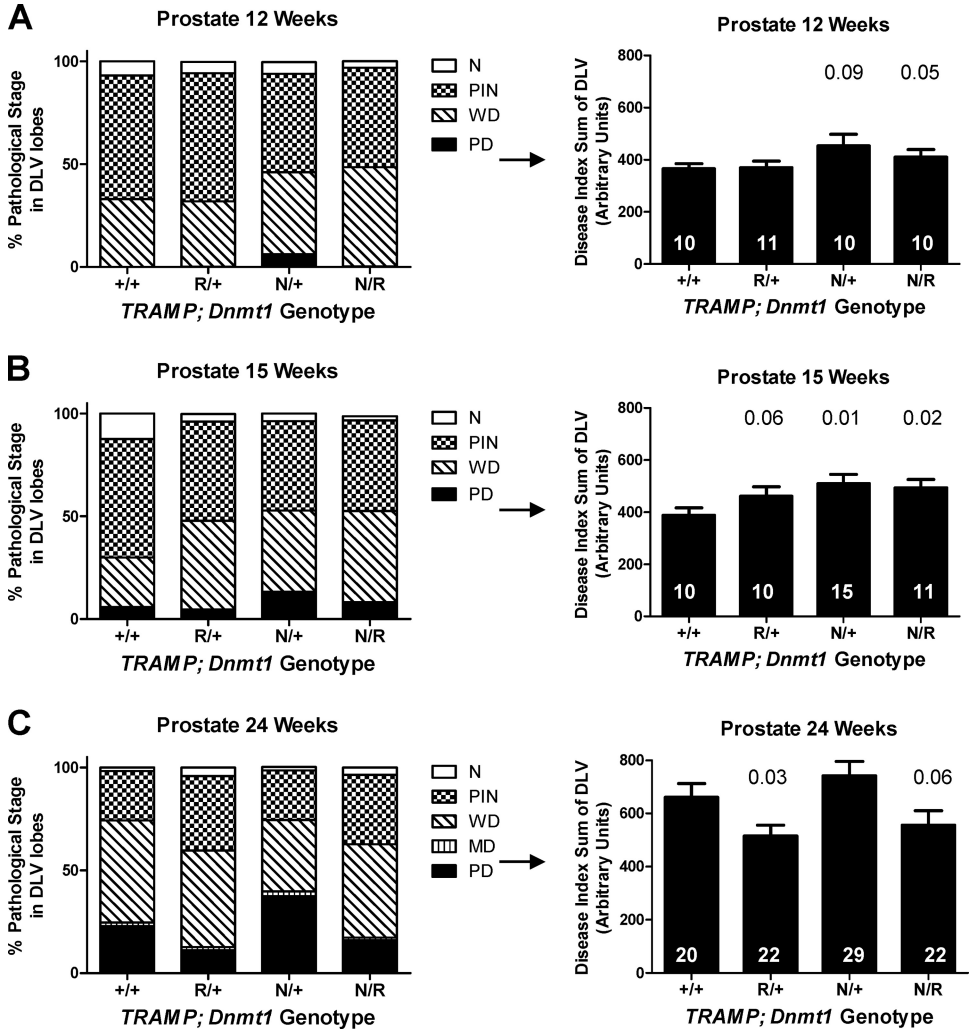

FIG. 9. Prostate pathological stage and disease index in *TRAMP*; *Dnmt1* hypomorphic mice. Pathological stage was determined for the dorsal, lateral, and ventral prostate lobes (DLV) and averaged as described in Materials and Methods. (A) The proportion of the prostate classified as normal (N), PIN, well-differentiated tumor (WD), moderately differentiated tumor (MD), and poorly differentiated tumor (PD) for mice of each TRAMP genotype, at 12 weeks of age, is plotted on the left. A disease index score was calculated as described in Materials and Methods and is plotted at right. The number of samples analyzed per group is indicated on the bars, and the means and standard errors are plotted. (B) Pathological staging and disease index score as described in panel A for 15-week-old mice. (C) Pathological staging and disease index score as described in panel A for 24-week-old mice. Mann-Whitney test P values of significant differences ($P \leq 0.09$), compared to *TRAMP*; $Dnmt1^{+/+}$ mice, are shown.

ease index score). Global DNA hypomethylation was also observed in *Dnmt1* hypomorphic mice at these time points. Thus, reduced Dnmt1 expression and the associated reduction in global DNA methylation appear to functionally alter the disease phenotype. Global DNA hypomethylation is associated with genomic instability and oncogene expression, both of which contribute to oncogenesis (9, 12, 22). Our data suggest that one or both of these mechanisms may contribute to tumorigenesis in TRAMP.

In direct contrast to the tumor-promoting effect seen at early ages in *TRAMP*; *Dnmt1* hypomorphic mice, at a later time point (24 weeks), these mice showed similar or slightly reduced primary prostate tumor incidence, as well as significantly decreased pathological stage (i.e., the disease index). These effects coincided with dramatic reductions in locus-specific DNA hypermethylation genome-wide, as revealed by HELP analyses. These observations support the notion that aberrant locus-specific DNA hypermethylation contributes to late stages of primary tumor development in TRAMP.

It should be noted that some of the changes in tumor phenotype observed here could be related to either strain or *Dnmt1* allele-specific effects. Because the experimental mice were not 100% FVB mice, this could affect the linkage for the $Dnmt1^{R}$ allele to the C57BL/6 strain, such that $Dnmt1^{R/+}$ and $Dnmt1^{N/R}$ mice may display phenotypic similarities that are based on strain and not genotype. In fact, there were a few instances where this appeared to occur, including the disease index scores at 24 weeks of age. A previous report utilizing the identical *Dnmt1* hypomorphic model revealed an analogous effect on tumor phenotype wherein $Dnmt1^{R/+}$ and $Dnmt1^{N/R}$

TABLE 5. Micrometastatic tumor incidence in *TRAMP*; *Dnmt1* hypomorphic mice[a]

Time (in wks) and TRAMP *Dnmt1* genotype	*n*	Local micrometastatic tumors		Distant micrometastatic tumors	
		%	*P*	%	*P*
12					
+/+	9	0	NA	0	NA
R/+	9	0	1	0	1
N/+	10	0	1	0	1
N/*R*	10	0	1	0	1
15					
+/+	10	0	NA	0	NA
R/+	9	0	1	0	1
N/+	15	13	0.5	0	1
N/*R*	11	9	1	0	1
24					
+/+	20	40	NA	15	NA
R/+	22	23	0.32	9	0.66
N/+	22	50	0.55	5	0.33
N/*R*	22	41	1	0	0.10

[a] As determined by IHC staining for large T antigen (Tag). "Local" refers to lymph node tumors; "distant" refers to liver, lung, or kidney tumors. Fisher exact test *P* values, compared to *TRAMP*; *Dnmt1*$^{+/+}$ mice, were determined. NA, not applicable. *n*, number of mice.

mice in the *Mlh1*$^{-/-}$ background sometimes showed effects distinct from that seen in *Dnmt1*$^{N/+}$ mice, despite the fact that experimental mice had been backcrossed for at least 10 generations to reduce strain variability (52). It is also possible that specific differences between the configuration of the *Dnmt1* R and N alleles could have distinct phenotypic effects (52). Nevertheless, in almost all instances, *TRAMP*; *Dnmt1*$^{N/R}$ mice, which have the most robust loss of Dnmt1 expression and DNA hypomethylation, also showed the most divergent molecular and biological phenotypes, confirming the validity of the model system.

Dnmt1 promotes prostate cancer metastasis. The most striking finding in the present study was the dramatic inhibition of prostate tumor metastases observed in *TRAMP*; *Dnmt1*$^{N/R}$ mice. While approximately one-third of control mice displayed macrometastatic tumor growth at 24 weeks of age, no lesions were observed in *TRAMP*; *Dnmt1*$^{N/R}$ mice. Moreover, clear reduction of macrometastatic tumors occurred in the other hypomorphic *TRAMP*; *Dnmt1* strains. The reduced level of macrometastases corresponded to both local and distant site tumors. In contrast to the effect on macrometastases, IHC staining for Tag-positive cells (scored as micrometastases) revealed similar levels of local (lymph node) involved micrometastatic tumors in control and *Dnmt1* hypomorphic mice. These data suggest that the early stages of metastases, e.g., invasion and colonization of the draining lymph nodes, are not inhibited by Dnmt1 reduction. Rather, it is the growth of these microscopic metastatic lesions at secondary sites that appears to be impacted. In light of our data, it is notable that numerous studies suggest that growth of macroscopic foci at distant sites is the rate-limiting step in tumor metastases (8).

Importantly, *TRAMP*; *Dnmt1* hypomorphic mice showed reduced levels of micrometastatic tumor growth at distant organs (i.e., liver, lung, and kidney). This effect was most dramatic in *TRAMP*; *Dnmt1*$^{N/R}$ mice, in which no distant site micrometastatic lesions were detected. Taken together, our data suggest that Dnmt1 contributes to at least two different stages of prostate metastasis: (i) the growth of already present micrometastatic lesions in the lymph nodes and (ii) the colonization and growth of metastases at distant organs. As with other solid tumors, metastasis is the key event conferring poor prognosis in human prostate cancer (13); thus, identification of factors that contribute to this process, such as Dnmt1, is critically important.

In agreement with our findings, Day and coworkers have shown that treatment of intact or castrated TRAMP mice with the DNA methyltransferase inhibitor 5-aza-2′-deoxycytidine (DAC) inhibits both primary tumor growth and the development of lymph node macrometastases (34, 56). While DAC has effects beyond inhibition of DNA methylation, the data suggest that inhibition of DNA hypermethylation mediated by Dnmt1 may be directly responsible for the phenotypes observed in the current and prior studies. The data showing that robust DNA hypermethylation occurs in late-stage prostate cancer, castration-recurrent prostate cancer, and metastatic prostate cancer in both mouse models and humans also support this idea (2, 35, 37, 38). Moreover, studies using *in vitro* cell models suggest that aberrant DNA methylation mediated by Dnmt enzymes contributes to the development of cellular phenotypes associated with metastasis (5, 30, 40, 54, 55). It will be of particular importance to define the genes targeted by DNA hypermethylation that contribute to prostate cancer metastasis.

In summary, based on our earlier characterization of the

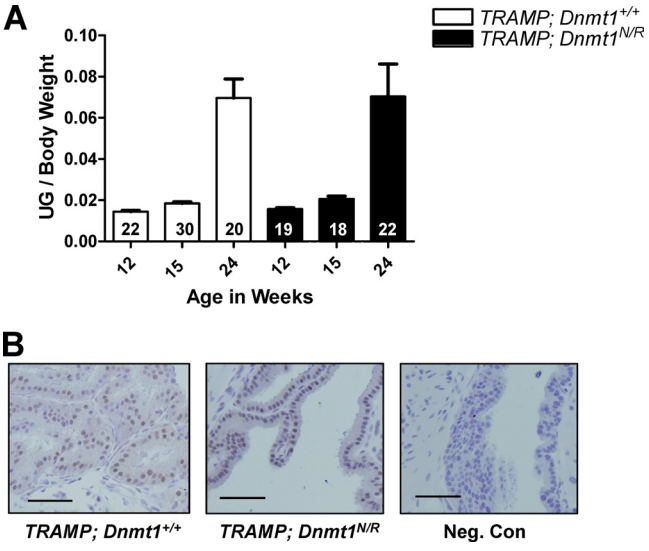

FIG. 10. Urogenital tract (UG) weight and androgen receptor (AR) staining in *TRAMP*; *Dnmt1*$^{+/+}$ and *TRAMP*; *Dnmt1*$^{N/R}$ mice. (A) UG weight normalized to body weight. The number of samples analyzed per group is indicated on the bars, and the means and standard errors are plotted. No significant differences between the two genotypes ($P \leq 0.05$; Mann-Whitney test) were observed. (B) Representative example of AR IHC staining in the seminal vesicles of 24-week-old mice of the indicated genotypes. IHC was performed as described in Materials and Methods, and the negative control is shown at right. Scale bar, 100 μm.

epigenetic changes during TRAMP tumorigenesis, we hypothesized that Dnmt1 may play a dual role in prostate caner progression characterized by tumor suppressor activity during early stages of the disease and oncogenic function at late stages. Our findings from the *TRAMP*; *Dnmt1* hypomorphic mouse model confirm this hypothesis and suggest that Dnmt1 has opposing effects on early and late stage prostate cancer. Importantly, the apparent tumor-promoting effect of Dnmt reduction on early-stage lesions in *Dnmt1* hypomorphic mice does not support the use of DNA hypomethylating agents as chemopreventive approaches for prostate cancer. However, the robust inhibitory effect of Dnmt1 reduction on prostate tumor metastasis (and in particular the prominent reduction of distant-site metastasis), which constitutes the clinically relevant human condition, is striking. This outcome supports further investigation of Dnmt1 inhibitors as therapeutic interventions for advanced and metastatic prostate cancer.

ACKNOWLEDGMENTS

This study was supported by NIH R21CA128062 (A.R.K.), Roswell Park Alliance Foundation (A.R.K.), 5T32CA009072 (S.R.M.K.), DOD PC060354 (S.R.M.K.), and NCI Center Grant (CA16056) (Roswell Park Cancer Institute [RPCI]).

We thank Petra Link of the Karpf lab and Ellen Karasik and Bryan Gillard of the RPCI Mouse Tumor Model Core for outstanding technical support. We thank Peter Laird (USC) for generously providing *Dnmt1* hypomorphic mice and for valuable advice and David Goodrich (RPCI) for numerous helpful suggestions.

REFERENCES

1. **Baba, S., Y. Yamada, Y. Hatano, Y. Miyazaki, H. Mori, T. Shibata, and A. Hara.** 2009. Global DNA hypomethylation suppresses squamous carcinogenesis in the tongue and esophagus. Cancer Sci. **100:**1186–1191.
2. **Camoriano, M., S. R. Kinney, M. T. Moser, B. A. Foster, J. L. Mohler, D. L. Trump, A. R. Karpf, and D. J. Smiraglia.** 2008. Phenotype-specific CpG island methylation events in a murine model of prostate cancer. Cancer Res. **68:**4173–4182.
3. **Cooper, C. S., and C. S. Foster.** 2009. Concepts of epigenetics in prostate cancer development. Br. J. Cancer **100:**240–245.
4. **Dehm, S. M., and D. J. Tindall.** 2007. Androgen receptor structural and functional elements: role and regulation in prostate cancer. Mol. Endocrinol. **21:**2855–2863.
5. **Deng, T., Y. Kuang, L. Wang, J. Li, Z. Wang, and J. Fei.** 2009. An essential role for DNA methyltransferase 3a in melanoma tumorigenesis. Biochem. Biophys. Res. Commun. **387:**611–616.
6. **De Smet, C., C. Lurquin, B. Lethe, V. Martelange, and T. Boon.** 1999. DNA methylation is the primary silencing mechanism for a set of germ line- and tumor-specific genes with a CpG-rich promoter. Mol. Cell. Biol. **19:**7327–7335.
7. **Eads, C. A., A. E. Nickel, and P. W. Laird.** 2002. Complete genetic suppression of polyp formation and reduction of CpG-island hypermethylation in $Apc^{Min/+}$ Dnmt1-hypomorphic Mice. Cancer Res. **62:**1296–1299.
8. **Eccles, S. A., and D. R. Welch.** 2007. Metastasis: recent discoveries and novel treatment strategies. Lancet **369:**1742–1757.
9. **Eden, A., F. Gaudet, A. Waghmare, and R. Jaenisch.** 2003. Chromosomal instability and tumors promoted by DNA hypomethylation. Science **300:**455.
10. **Ehrich, M., M. R. Nelson, P. Stanssens, M. Zabeau, T. Liloglou, G. Xinarianos, C. R. Cantor, J. K. Field, and D. van den Boom.** 2005. Quantitative high-throughput analysis of DNA methylation patterns by base-specific cleavage and mass spectrometry. Proc. Natl. Acad. Sci. U. S. A. **102:**15785–15790.
11. **Esteve, P. O., H. G. Chin, A. Smallwood, G. R. Feehery, O. Gangisetty, A. R. Karpf, M. F. Carey, and S. Pradhan.** 2006. Direct interaction between DNMT1 and G9a coordinates DNA and histone methylation during replication. Genes Dev. **20:**3089–3103.
12. **Feinberg, A. P., and B. Tycko.** 2004. The history of cancer epigenetics. Nat. Rev. Cancer **4:**143–153.
13. **Foley, C. L., and M. R. Feneley.** 2009. The clinical significance and therapeutic implications of extraprostatic invasion. Surg. Oncol. **18:**203–212.
14. **Gaudet, F., J. G. Hodgson, A. Eden, L. Jackson-Grusby, J. Dausman, J. W. Gray, H. Leonhardt, and R. Jaenisch.** 2003. Induction of tumors in mice by genomic hypomethylation. Science **300:**489–492.
15. **Gingrich, J. R., R. J. Barrios, R. A. Morton, B. F. Boyce, F. J. DeMayo, M. J. Finegold, R. Angelopoulou, J. M. Rosen, and N. M. Greenberg.** 1996. Metastatic prostate cancer in a transgenic mouse. Cancer Res. **56:**4096–4102.
16. **Greenberg, N. M., F. DeMayo, M. J. Finegold, D. Medina, W. D. Tilley, J. O. Aspinall, G. R. Cunha, A. A. Donjacour, R. J. Matusik, and J. M. Rosen.** 1995. Prostate cancer in a transgenic mouse. Proc. Natl. Acad. Sci. U. S. A. **92:**3439–3443.
17. **Guo, Z. S., J. A. Hong, K. R. Irvine, G. A. Chen, P. J. Spiess, Y. Liu, G. Zeng, J. R. Wunderlich, D. M. Nguyen, N. P. Restifo, and D. S. Schrump.** 2006. De novo induction of a cancer/testis antigen by 5-aza-2′-deoxycytidine augments adoptive immunotherapy in a murine tumor model. Cancer Res. **66:**1105–1113.
18. **Hurwitz, A. A., B. A. Foster, J. P. Allison, N. M. Greenberg, and E. D. Kwon.** 2001. The TRAMP mouse as a model for prostate cancer. Curr. Protoc. Immunol. **Chapter 20:**Unit 20.5.
19. **Jair, K. W., K. E. Bachman, H. Suzuki, A. H. Ting, I. Rhee, R. W. Yen, S. B. Baylin, and K. E. Schuebel.** 2006. De novo CpG island methylation in human cancer cells. Cancer Res. **66:**682–692.
20. **Kaplan-Lefko, P. J., T. M. Chen, M. M. Ittmann, R. J. Barrios, G. E. Ayala, W. J. Huss, L. A. Maddison, B. A. Foster, and N. M. Greenberg.** 2003. Pathobiology of autochthonous prostate cancer in a pre-clinical transgenic mouse model. Prostate **55:**219–237.
21. **Karpf, A. R., and D. A. Jones.** 2002. Reactivating the expression of methylation silenced genes in human cancer. Oncogene **21:**5496–5503.
22. **Karpf, A. R., and S. Matsui.** 2005. Genetic disruption of cytosine DNA methyltransferase enzymes induces chromosomal instability in human cancer cells. Cancer Res. **65:**8635–8639.
23. **Karpf, A. R., B. C. Moore, T. O. Ririe, and D. A. Jones.** 2001. Activation of the p53 DNA damage response pathway after inhibition of DNA methyltransferase by 5-aza-2′-deoxycytidine. Mol. Pharmacol. **59:**751–757.
24. **Khulan, B., R. F. Thompson, K. Ye, M. J. Fazzari, M. Suzuki, E. Stasiek, M. E. Figueroa, J. L. Glass, Q. Chen, C. Montagna, E. Hatchwell, R. R. Selzer, T. A. Richmond, R. D. Green, A. Melnick, and J. M. Greally.** 2006. Comparative isoschizomer profiling of cytosine methylation: the HELP assay. Genome Res. **16:**1046–1055.
25. **Kim, E. K., J. Y. Kang, Y. H. Rho, Y. S. Kim, D. S. Kim, and Y. S. Bae.** 2009. Silencing of the CKIIα and CKIIα′ genes during cellular senescence is mediated by DNA methylation. Gene **431:**55–60.
26. **Kincl, F. A., M. Maqueo, and R. I. Dorfman.** 1965. Influence of various steroids on testes and accessory sex organs in the rat. Acta Endocrinol. **49:**145–154.
27. **Laird, P. W., L. Jackson-Grusby, A. Fazeli, S. L. Dickinson, W. E. Jung, E. Li, R. A. Weinberg, and R. Jaenisch.** 1995. Suppression of intestinal neoplasia by DNA hypomethylation. Cell **81:**197–205.
28. **La Salle, S., C. Mertineit, T. Taketo, P. B. Moens, T. H. Bestor, and J. M. Trasler.** 2004. Windows for sex-specific methylation marked by DNA methyltransferase expression profiles in mouse germ cells. Dev. Biol. **268:**403–415.
29. **Li, E., T. H. Bestor, and R. Jaenisch.** 1992. Targeted mutation of the DNA methyltransferase gene results in embryonic lethality. Cell **69:**915–926.
30. **Lin, R. K., C. H. Hsu, and Y. C. Wang.** 2007. Mithramycin A inhibits DNA methyltransferase and metastasis potential of lung cancer cells. Anticancer Drugs **18:**1157–1164.
31. **Link, P. A., M. R. Baer, S. R. James, D. A. Jones, and A. R. Karpf.** 2008. p53-inducible ribonucleotide reductase (p53R2/RRM2B) is a DNA hypomethylation-independent decitabine gene target that correlates with clinical response in myelodysplastic syndrome/acute myelogenous leukemia. Cancer Res. **68:**9358–9366.
32. **Lucarelli, M., A. Fuso, R. Strom, and S. Scarpa.** 2001. The dynamics of myogenin site-specific demethylation is strongly correlated with its expression and with muscle differentiation. J. Biol. Chem. **276:**7500–7506.
33. **Mavis, C. K., S. R. Morey Kinney, B. A. Foster, and A. R. Karpf.** 2009. Expression level and DNA methylation status of glutathione *S*-transferase genes in normal murine prostate and TRAMP tumors. Prostate **69:**1312–1324.
34. **McCabe, M. T., J. A. Low, S. Daignault, M. J. Imperiale, K. J. Wojno, and M. L. Day.** 2006. Inhibition of DNA methyltransferase activity prevents tumorigenesis in a mouse model of prostate cancer. Cancer Res. **66:**385–392.
35. **Morey Kinney, S. R., D. J. Smiraglia, S. R. James, M. T. Moser, B. A. Foster, and A. R. Karpf.** 2008. Stage-specific alterations of DNA methyltransferase expression, DNA hypermethylation, and DNA hypomethylation during prostate cancer progression in the transgenic adenocarcinoma of mouse prostate model. Mol. Cancer Res. **6:**1365–1374.
36. **Morey Kinney, S. R., W. Zhang, M. Pascual, J. M. Greally, B. Gillard, E. Karasik, B. A. Foster, and A. R. Karpf.** 2009. Lack of evidence for green tea polyphenols as DNA methylation inhibitors in murine prostate. Cancer Prevention Res. **2:**1065–1075.
37. **Morey, S. R., D. J. Smiraglia, S. R. James, J. Yu, M. T. Moser, B. A. Foster, and A. R. Karpf.** 2006. DNA methylation pathway alterations in an autochthonous murine model of prostate cancer. Cancer Res. **66:**11659–11667.
38. **Nelson, W. G., A. M. De Marzo, and S. Yegnasubramanian.** 2009. Epigenetic alterations in human prostate cancers. Endocrinology **150:**3991–4002.
39. **Oda, M., J. L. Glass, R. F. Thompson, Y. Mo, E. N. Olivier, M. E. Figueroa,**

R. R. Selzer, T. A. Richmond, X. Zhang, L. Dannenberg, R. D. Green, A. Melnick, E. Hatchwell, E. E. Bouhassira, A. Verma, M. Suzuki, and J. M. Greally. 2009. High-resolution genome-wide cytosine methylation profiling with simultaneous copy number analysis and optimization for limited cell numbers. Nucleic Acids Res. **37:**3829–3839.

40. **Olsson, L., and J. Forchhammer.** 1984. Induction of the metastatic phenotype in a mouse tumor model by 5-azacytidine, and characterization of an antigen associated with metastatic activity. Proc. Natl. Acad. Sci. U. S. A. **81:**3389–3393.
41. **Patra, S. K., A. Patra, and R. Dahiya.** 2001. Histone deacetylase and DNA methyltransferase in human prostate cancer. Biochem. Biophys. Res. Commun. **287:**705–713.
42. **Rai, K., L. D. Nadauld, S. Chidester, E. J. Manos, S. R. James, A. R. Karpf, B. R. Cairns, and D. A. Jones.** 2006. Zebra fish Dnmt1 and Suv39h1 regulate organ-specific terminal differentiation during development. Mol. Cell. Biol. **26:**7077–7085.
43. **Rauch, T., Z. Wang, X. Zhang, X. Zhong, X. Wu, S. K. Lau, K. H. Kernstine, A. D. Riggs, and G. P. Pfeifer.** 2007. Homeobox gene methylation in lung cancer studied by genome-wide analysis with a microarray-based methylated CpG island recovery assay. Proc. Natl. Acad. Sci. U. S. A. **104:**5527–5532.
44. **Robertson, K. D.** 2002. DNA methylation and chromatin: unraveling the tangled web. Oncogene **21:**5361–5379.
45. **Ropke, A., P. Buhtz, M. Bohm, J. Seger, I. Wieland, E. P. Allhoff, and P. F. Wieacker.** 2005. Promoter CpG hypermethylation and downregulation of DICE1 expression in prostate cancer. Oncogene **24:**6667–6675.
46. **Rozen, S., and H. Skaletsky.** 2000. Primer3 on the WWW for general users and for biologist programmers. Methods Mol. Biol. **132:**365–386.
47. **Schenk, T., S. Stengel, S. Goellner, D. Steinbach, and H. P. Saluz.** 2007. Hypomethylation of PRAME is responsible for its aberrant overexpression in human malignancies. Genes Chromosomes Cancer **46:**796–804.
48. **Schmittgen, T. D., and B. A. Zakrajsek.** 2000. Effect of experimental treatment on housekeeping gene expression: validation by real-time, quantitative RT-PCR. J. Biochem. Biophys. Methods **46:**69–81.
49. **Shen, L., Y. Kondo, Y. Guo, J. Zhang, L. Zhang, S. Ahmed, J. Shu, X. Chen, R. A. Waterland, and J. P. Issa.** 2007. Genome-wide profiling of DNA methylation reveals a class of normally methylated CpG island promoters. PLoS Genet. **3:**2023–2036.
50. **Song, L., S. R. James, L. Kazim, and A. R. Karpf.** 2005. Specific method for the determination of genomic DNA methylation by liquid chromatography-electrospray ionization tandem mass spectrometry. Anal. Chem. **77:**504–510.
51. **Thompson, R. F., M. Reimers, B. Khulan, M. Gissot, T. A. Richmond, Q. Chen, X. Zheng, K. Kim, and J. M. Greally.** 2008. An analytical pipeline for genomic representations used for cytosine methylation studies. Bioinformatics **24:**1161–1167.
52. **Trinh, B. N., T. I. Long, A. E. Nickel, D. Shibata, and P. W. Laird.** 2002. DNA methyltransferase deficiency modifies cancer susceptibility in mice lacking DNA mismatch repair. Mol. Cell. Biol. **22:**2906–2917.
53. **Yamada, Y., L. Jackson-Grusby, H. Linhart, A. Meissner, A. Eden, H. Lin, and R. Jaenisch.** 2005. Opposing effects of DNA hypomethylation on intestinal and liver carcinogenesis. Proc. Natl. Acad. Sci. U. S. A. **102:**13580–13585.
54. **Yaqinuddin, A., S. A. Qureshi, R. Qazi, and F. Abbas.** 2008. Down-regulation of DNMT3b in PC3 cells effects locus-specific DNA methylation, and represses cellular growth and migration. Cancer Cell Int. **8:**13.
55. **Yaqinuddin, A., S. A. Qureshi, R. Qazi, S. Farooq, and F. Abbas.** 2009. DNMT1 silencing affects locus specific DNA methylation and increases prostate cancer derived PC3 cell invasiveness. J. Urol. **182:**756–761.
56. **Zorn, C. S., K. J. Wojno, M. T. McCabe, R. Kuefer, J. E. Gschwend, and M. L. Day.** 2007. 5-Aza-2′-deoxycytidine delays androgen-independent disease and improves survival in the transgenic adenocarcinoma of the mouse prostate mouse model of prostate cancer. Clin. Cancer Res. **13:**2136–2143.